CHAPTER 9

ESTIMATION OF PROPAGATION IMPAIRMENTS

9.1 INTRODUCTION

Background material on the various propagation effects on satellite communications has been presented in previous chapters, and in this chapter further attention is devoted to consideration of the magnitudes of the effects for use in system design. Illustrative numerical examples are given. The phenomena are treated in essentially the same order as in Chaps. 1 through 7. Thus ionospheric effects are considered first. Table 9.1 (same as Table 2.2) provides a summary of ionospheric effects (not including ionospheric scintillation).

9.2 IONOSPHERIC EFFECTS

9.2.1 Faraday Rotation: Determination of Longitudinal Component of Magnetic Field.

Many satellite communication systems employ circularly polarized waves and therefore need not be concerned about Faraday rotation. Some satellites transmit linearly polarized waves which are subject to Faraday rotation, however, and attention is given here to its estimation. One reason for using linearly polarized transmission may be to obtain information about ionospheric total electron content (TEC) which contributes to excess range delay and other effects in addition to Faraday rotation. At high frequencies, Faraday rotation along a path is given in S1 units by

$$\phi = \frac{2.36 \times 10^4}{f^2} \int N B \cos\theta_B \, dl \qquad \text{rad} \qquad (9.1)$$

where ϕ is the Faraday rotation angle in radians, f is frequency in Hz, N is electron densityin electrons/m^3 (el/m^3), B is magnetic flux density of the Earth's field, and θ_B is the angle between the path and the B vector. The S1 unit for B is the tesla (T), also commonly referred to as Webers/m^2 (Wb/m^2). Evaluation of the integral involves the values of N, B, and cos θ_B along the path, but

for some situations, for geostationary and orbiting earth satellites, it is sufficiently accurate to replace B cos θ_B by an average or effective value $\bar{B}_L$ and take it outside the integral. Then the relation has the form of

$$\phi = \frac{2.36 \times 10^4 \bar{B}_L}{f^2} \int N\,dl = \frac{2.36 \times 10^4 \bar{B}_L}{f^2} \text{ (TEC) rad} \quad (9.2)$$

where

$$\bar{B}_L \quad \frac{\int N B \cos\theta_B\, dl}{\int N\, dl} \quad \text{T or Wb/m}^2 \quad (9.3)$$

Table 9.1 Estimated maximum ionospheric effects in the United States for one-way paths at an elevation angle of 30 deg (same as Table 2.2).

Effect	100 MHz	300 MHz	1 GHz	3 GHz	10 GHz
Faraday rotation	30 rot.	3.3 rot.	108°	12°	1.1°
Excess time delay	25 μs	2.8 μs	0.25 μs	0.028 μs	0.0025 μs
Refraction	≤ 1°	<7 min	≤0.6 min	<4.2 s	≤0.36 s
Variation in direction of arrival	20 min	2.2 min	.12 s	1.32 s	0.12 s
Absorption (auroral and polar cap)	5 dB	1.1 dB	0.05 dB	6×10^{-3} dB	5×10^{-4} dB
Absorption (mid latitude)	<1 dB	0.1 dB	<0.01 dB	$<1\times10^{-3}$ dB	$<10^{-4}$ dB
Dispersion	0.4 ps/Hz	0.015 ps/Hz	0.0004 ps/Hz	1.5×10^{-5} ps/Hz	4×10^{-7} ps/Hz

A variation of this procedure has been employed by Davies who used

$$\phi = \frac{8.44 \times 10^{-7}}{f^2} \int f_L \, N \, dl \qquad \text{rad}$$

$$\phi = \frac{8.44 \times 10^{-7}}{f^2} \, \bar{F} \, (TEC) \qquad \text{rad} \qquad (9.4)$$

with $\bar{F}$ defined by

$$\bar{F} = \frac{\int N f_H \cos \theta_B \, dl}{\int N \, dl} \qquad (9.5)$$

As the electron gyrofrequency f_H in Hz equals 2.8 x 1010 B and (2.8 x 10^{10}) X (8.44 x 10^{-7}) = 2.36 x 104, the two variations are seen to be compatible. The values of TEC obtained by use of Eqs. (9.2) and (9. 4) are values for slant paths. If it desired to determine TEC values for equivalent vertical paths, one may use

$$\phi = \frac{2.36 \times 10^{4}}{f} \, \bar{M} \, (TEC) \qquad \text{rad} \qquad (9.6)$$

with

$$\bar{M} = \frac{\int N B \cos \theta_B \sec \chi \, dh}{\int N \, dh} \qquad (9.7)$$

where χ is the zenith angle and dh represents an element of length in the vertical direction (Titheridge, 1972). Davies (1980) has pointed out that the use of an effective vertical content is advantageous when comparing contents over different paths but may be somewhat misleading because there may be no existing vertical path that has the inferred vertical content.

Equations (9.3), (9. 5), and (9.7) show what the values of $\bar{B}_L$, $\bar{F}$, and $\bar{M}$ represent but in practice it is generally considered that for" $\bar{B}_L$, for example, the value of B_L (B cos θ_B) at a height such as 400 or 420 km represents a sufficiently good approximation to $\bar{B}_L$

The approach to be used to estimate Faraday rotation depends on the degree of accuracy required. If only a very rough estimate is needed one may refer to Table 9.1 or Fig. 9.1 if an estimate of TEC is available, If somewhat greater accuracy is needed, it may be advisable to determine a value for B_L for the path and to then use Eq. (9.2) for calculating Faraday rotation as a function of TEC. In determining B_L, one has a choice of using a simple dipole model of the Earth's field or more sophisticated models, The dipole model is useful for preliminary estimates or when finding, facilities, or location do not justify the use of more accurate models. The need for a more accurate model than the dipole model tends to be greater at low geomagnetic latitudes than at the higher latitudes. It should be recognized in any case that Faraday rotation is proportional to ionospheric TEC, which is highly variable, and high accuracy in determining B_L may not be justifiable. Also the use of a fixed value of B_L introduces errors and if the highest precision is desired one should theoretical y evaluate Faraday rotation by using the integral formulation or by use of a summation obtained by separating the ionosphere into layers of known or assumed values of N, B, and cos θ_B.

The view is taken here that it is useful in some cases to use the value for B_L at 400 km obtained by using a dipole model for the Earth's field, and a procedure for doing so is presented as Appendix - 9.1. If one wishes to be assured of greater accuracy than about 25 percent for determining B_L, one can make use of the spherical harmonic coefficients of the International Geomagnetic Reference Field (EOS, June 17, 1986) and a computer algorithm for synthesizing the geomagnetic field such as that by Malin and Barraclough (198 1). A special issue of the Journal of Geomagnetism and Geoelecticity (vol. 34, no. 6, 1982) was devoted to the international field. Also the Environmental Data and Information Service (EDIS) of NOAA, Boulder, Colorado can supply values of B_L based on the International Geomagnetic Reference Field. The following Example 9.1, however, illustrates the calculation of B_L at 400 km using a dipole model, The example uses the procedure of Appendix 9.1.

Example 9.1 Determination of B_L

Considering an earth station at Fairbanks, Alaska (65 deg N, 148 deg W) and a geostationary satellite at 148 deg W (on the same geographic meridian), this example illustrates how to find a value for B_L for evaluating Faraday rotation, using the dipole model of the Earth's field. In the example the geographic coordinates of the intersection of the dipole axis and the Earth's surface in the northern hemisphere are taken as 78.8 deg N and 70,9 deg W (Dawson and Newitt, 1982).

From Eqs. (A9. 17) and (9. 18) with $\theta'_g = 65°$, $\theta'_p = 78.8°$, and $\phi_g - \phi_p$ $148° - 70.9° = 77.1°$,

θ'_m 63.279° N (geomagnetic latitude)

ϕ_m – 66.373° W (geomagnetic longitude)

Using the procedure described with the aid of Fig. A9. 1 and Eq. (A9 ."1 4), the path from the earth station to the-satellite is found to intercept the 400-km level at a latitude of 56,013 deg N. The geomagnetic coordinates of this point, found by using Eqs. (A9. 17) and (A9. 18) again, now with $\theta'_g = 56.013$ deg, are

$\theta'_m = 56{,}889°$ N

$\phi_m = 85.94S°$ W

From Eqs. (A9.3), (A9.5), and (A9.6), using B_0 as 0.32 G (10,000 G = 1 Wb/m^2) and a/r= 6378/(6378 + 400),

H = 0.141 G, Z = 0.433 G, F = 0.455 G

and

$F = 0.433\ a_r + 0.146\ a_\theta$

Converting to rectangular coordinates by using Eqs. (A9.20) and (A9.21)

$F = 0.0251\ ax + 0.354\ a_y + 0.286\ a_z$

Next one needs to determine d = S - G, where S is the geostationary satellite position and G is the earth-station position. For S, θ'_m = 2.485 deg and ϕ = 77.338 deg from Eqs. (A9.17) and (A9.18), with θ'_o = O deg. Measuring distances in earth radii with the satellite at 6.6 radii and expressing in rectangular coordinates by use of Eqs. (A9.22 - A9.24),

$$s = 1.445\ a_x + 6.433\ a_y + 0.286\ a_z$$

For G, θ'_m = 63.279° and ϕ_m = 66.373° and, with G at a distance of 1 earth radius from the center of the Earth,

$$G = 0.180\ a_x + 0.412\ a_y + 0.893\ a_z$$

Then for d = S - G one obtains

$$d = 1.265\ a_x + 6.021\ a_y - 0.607\ a_z$$

Next using $F \cdot d = Fd \cos \theta_B$

$$1.988 = 2.813 \cos \theta_B$$

$$\cos \theta_B = 0.707,\ \theta_B = 45.03°.$$

Finally

$$'L = F \cos \theta_B = 0.322\ G = 3.22 \times 10^{-5}\ Wb/m^2.$$

In this example the earth station and satellite are at the same longitude. If they are not, Eqs. (A9. 15) and (A9. 16) and the adjacent explanation can be used to find the latitude and longitude of the 400-km intercept.

9.2.2 Propagation Effects Directly Dependent on TEC

The total electron content (TEC) along a path is the number of electrons in a column one square meter in cross section (electrons/m^2 or el/m^2) that coincides in position with the path. The TEC of the ionosphere has a pronounced diurnal variation as illustrated in Fig. 2.6 and also varies with solar activity, especially with geomagnetic storms which may result from solar activity. Faraday rotation, excess time delay and associated range

delay, phase advance, and time-delay and phase-advance dispersion are directly proportional to TEC. Most ionospheric effects, in fact, tend to be proportional to TEC.

9.2.2.1 Faraday Rotation

The angle of Faraday rotation is proportional to TEC as indicated by Eq. 9.2, which is repeated below. The theory of Faraday rotation was developed in Sec. 2.2, and Eq. 9.2 was further justified in Sec. 9.2.1 which was devoted primarily to consideration of B_L, the longitudinal component of the Earth's magnetic field.

$$\phi = \frac{2.36 \times 10^4}{f^2} B_L \text{ TEC}$$

For systems using linear polarization, uncompensated Faraday rotation can cause a polarization mismatch loss of 20 log δ, where $\delta = \cos \theta_i$ and θ_i is the polarization mismatch angle. This angle may equal the Faraday rotation angle ϕ but may also be less than ϕ, if a certain value of ϕ was anticipated and compensated for but the actual value of # was different. In addition to the diurnal variations of Faraday rotation and the variations with the solar cycle, rapid variations, having periods of fractions of a minute, are also sometimes observed. At Ascension Island at the equatorial anomaly crest, rapid variations of about 90 deg at 136 MHz were observed. at the same time that intense scintillation was recorded on 1.54 GHz MARISAST transmissions (Lee et al., 1982). Although Faraday rotation can sometimes be troublesome or at least must be taken into account to ensure satisfactory system performance, it can be a valuable tool for determining ionospheric TEC which causes excess time delay that is important to radionavigation and positioning satellite systems. Representative values of Faraday rotation are shown in Fig. 9.1 as a function of frequency and TEC.

9.2.2.2 Excess Time and Range Delay

The excess time delay At due to the TEC along a path is given by

$$\text{At} = \frac{40.3 \text{ TEC}}{cf^2} \left(\frac{1.34 \times 10^{-7} \text{ TEC}}{f^2} \right) \text{ s} \qquad (9.8)$$

and the excess range delay AR due to the TEC is specified by

$$AR = (40.3/f^2)\,TEC \qquad (9,9)$$

In Eqs. (9.8) and (9.9), f is frequency in Hz and TEC is total electron content in el/m^2. It is evident that determination of At and AR requires information about TEC.

Figure 9.2 shows time and range delay as a function of frequency for a one-way path for TEC values of 10^{17} and 1018 el/m^2. Sometimes a known or estimated value of TEC is available for a vertical path and it is desired to estimate delay for a path as a function of elevation angle, Figure 9.3 shows the excess range delay or error as a function of elevation angle for a TEC of 1018 el/m^2 on a vertical path for frequencies of 100 MHz, 400 MHz, and 1200 MHz (Millman, 1 980).

9.2.2.3 Phase Advance

The phase advance $\Delta\phi$ of an electromagnetic wave with respect to the value of phase for propagation through a vacuum is also directly proportional to TEC as expressed by

$$\Delta\phi = \frac{8.44 \times 10^{-7}}{f}\,TEC \quad \text{rad} \qquad (9.10)$$

The change in phase associated with a change in TEC may be of interest. For example, one may wish to relate the change in phase due to a traveling ionospheric disturbance (TID) to the change in TEC. Usin $\delta\phi$ for the change in phase associated with an increment $\Delta(TEC)$ in# C,

$$\delta\phi = \frac{8.44 \times 10^{-7}}{f}\,\Delta(TEC) \quad \text{rad} \qquad (9.11)$$

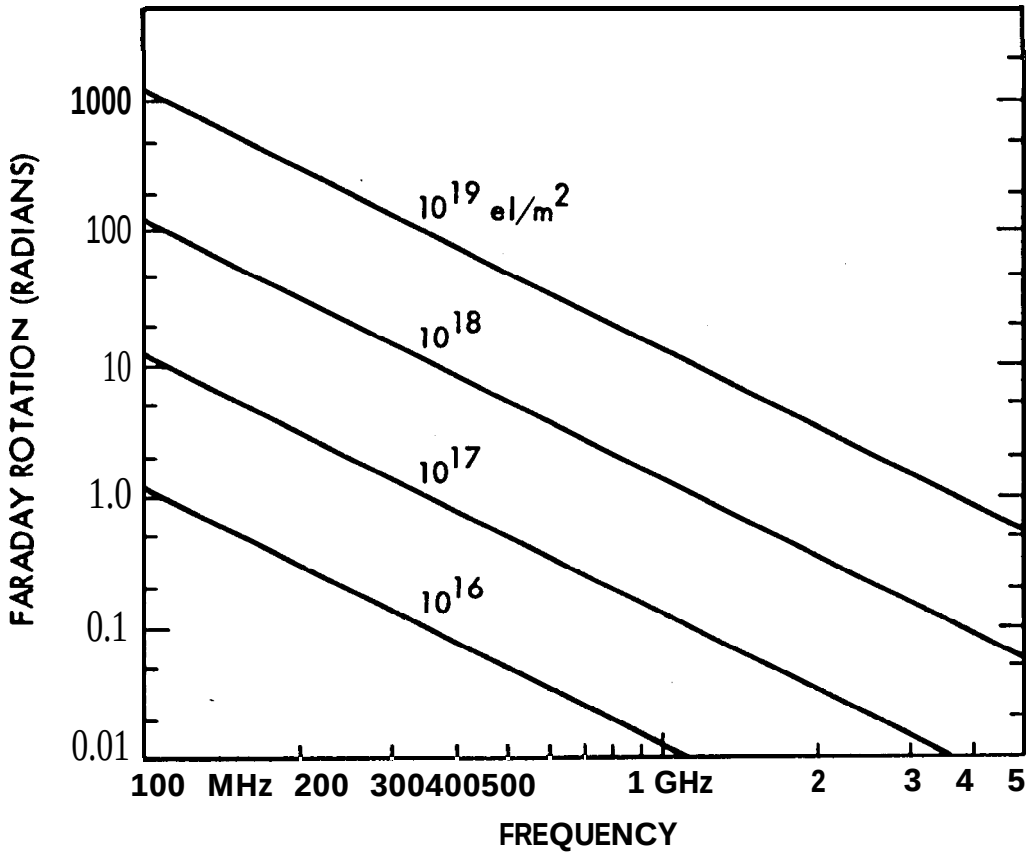

Figure 9.1. Faraday rotation as a function of ionospheric TEC and frequency (Klobuchar, 1978).

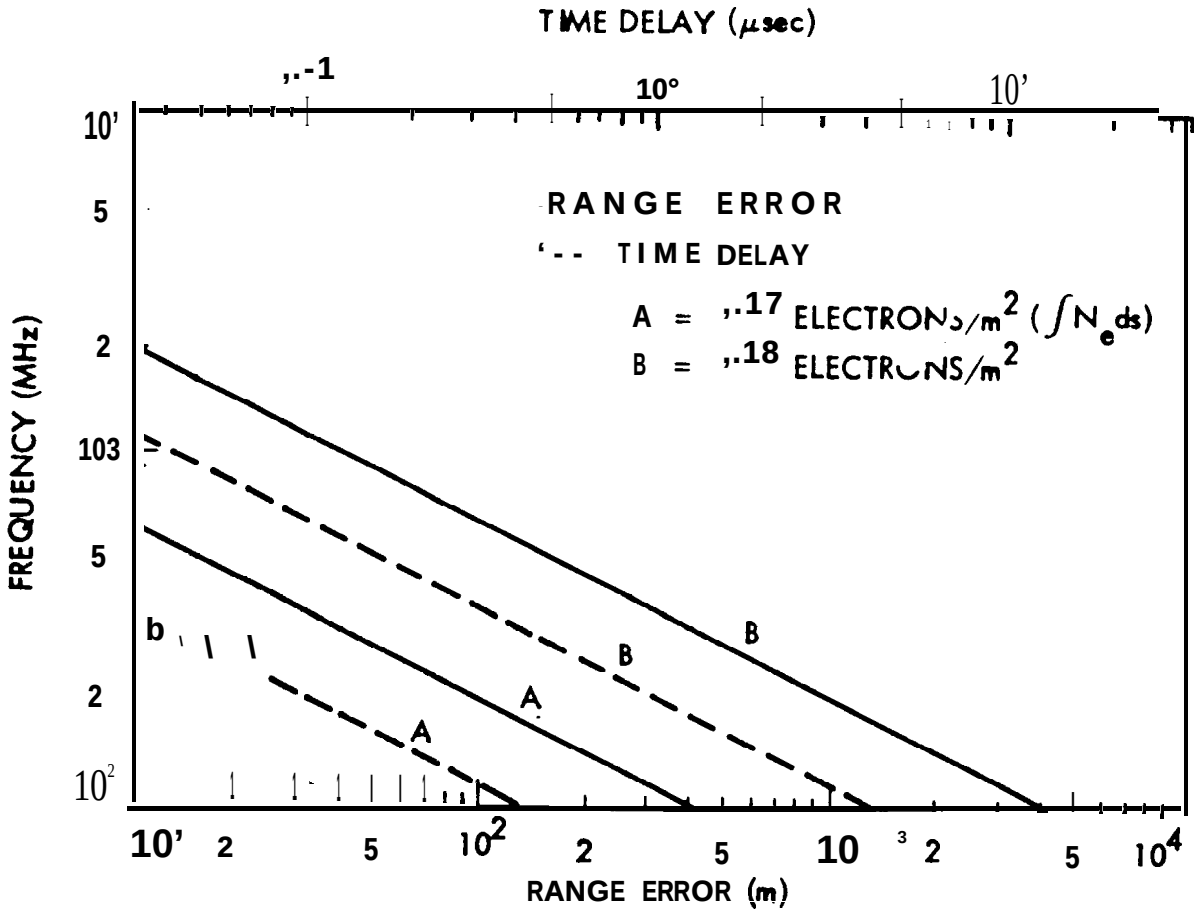

Figure 9.2. Ionospheric range error and time delay for a one-way path (Millman, 1980).

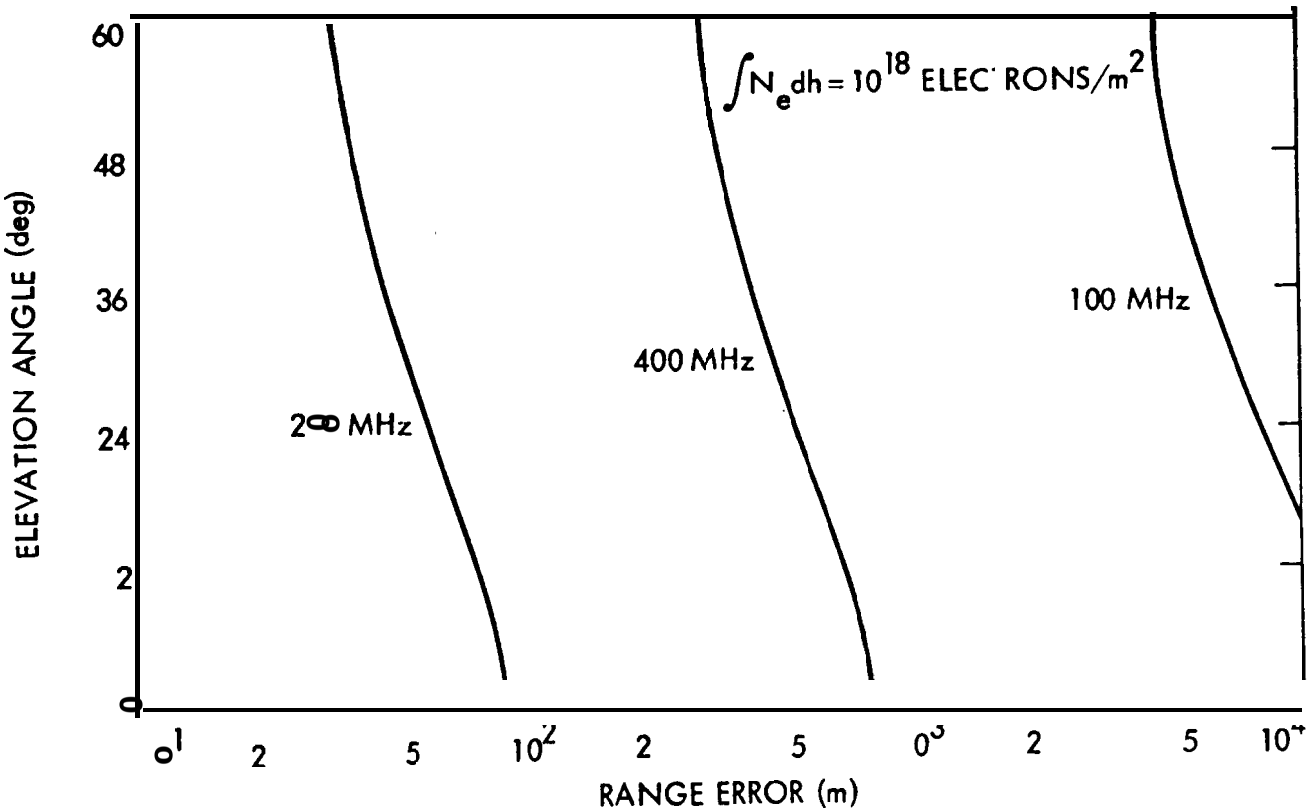

Figure 9.3. Ionospheric range error as a function of elevation angle and frequency (Millman, 1980).

9.2.2.4 Doppler Frequency

Frequency f and phase #1 are related by $f = (1/2\pi)(d\phi/dt)$, and the Doppler shift in frequency f_D associated with a change in phase due to variation of TEC with time is given by

$$f_D = \frac{1.34 \times 10^{-7}}{f} \frac{d(TEC)}{dt} \quad \text{Hz} \qquad (9.12)$$

The average Doppler frequency during a time interval or count time T_c in which TEC changes by $\Delta(TEC)$ is given by

$$f_D = \frac{1.34 \times 10^{-7}}{f} \frac{\Delta(TEC)}{T_c} \quad \text{Hz} \qquad (9.13)$$

9.2.2.5 Dispersion

The rate of change of time delay with frequency, referred to as time-delay dispersion, is

$$\frac{dt}{df} = -\frac{2.68 \times 10^{-7}}{f^3} TEC \quad \text{s/Hz} \qquad (9.14)$$

Applied to a pulse of length τ for which the associated bandwidth $\Delta f = 1/\tau$, the difference in time delay Δt between the two extreme frequencies of the pulse is given by

$$\Delta t = -\frac{2.68 \times 10^{-7}}{f^3} \Delta f\ (TEC) \quad \text{s} \qquad (9.15)$$

The effect of dispersion on a pulse propagating through the ionosphere is to decrease the amplitude, increase the length, and introduce frequency modulation (Millman, 1980). Whether the effects are of significance or not depends on the values of f, Δf, and TEC.

9.2.2.6 Refractive Bending

It develops that the refractive bending or change in direction of a ray traversing the ionosphere is proportional to TEC also. The expression given by Millman and ReinSmith (1974) for the elevation

angle error $\Delta\theta$ for a satellite for which the range R inconsiderably larger than r. sin θ_o, where r. is earth radius and. θ_o is elevation angle, is

$$\Delta\theta = (\cos\theta_o / 2h_i)\,AR \quad \text{rad} \qquad (9.16)$$

The quantity h_i is the height where the median electron content occurs and is generally between 300 and 450 km. As AR is the range error along the path and is proportional to TEC, $\Delta\theta$ is also proportional to TEC.

As irregularities in electron density such as those caused by TID's move across the line of sight and cause variations in TEC, the variations are reflected in ΔR and $\Delta\theta$.

9.2.2.7 Prediction and Measurement of TEC

TEC along a path is highly variable and difficult to predict accurately, but advance estimates or predictions of TEC may be needed for system planning and in system operations. Techniques are available for measuring TEC and these will be mentioned shortly, but their cost may preclude their use in some cases.

For some purposes it may be sufficient to estimate the maximum Faraday rotation or excess range delay that may be encountered. To obtain this estimate one may assume a maximum TEC of 10^{18} el/m^2 for a one-way zenith path (CCIR, 1986a). At night the value of TEC may drop to about one eigth of the maximum value. Figure 9.3 illustrates how effects proportional to TEC will tend to vary as a function of elevation angle θ in the range from O deg to 60 deg. When the value of TEC is given without qualification it normally refers to the zenith value, but the content along a slant path is often what is wanted. This value is commonly assumed to be the zenith value multiplied by the secant of the zenith angle at an ionospheric height h somewhat above that of the F layer maximum, thus taking into account the preponderence of ionization on the topside of the layer. A relation giving the zenith angle χ in terms of the elevation angle θ of the path at the surface is

$$\chi = \sin^{-1}\left(\frac{r_o}{r_o + h}\cos\theta\right) \qquad (9.17)$$

where r_o is the Earth's radius and h is ionospheric height, commonly 300 to 400 km. For example if θ = 30 deg and h = 350 km

$$\chi = \sin^{-1}\left[\frac{6371}{6371 + 350}(0.866)\right] \quad 55.18°$$

As a result sec χ = 1.75 and TEC for the slant path equals about 1.75 times the value for a zenith path.

The problem of predicting time delay due to TEC was considered carefully by Klobuchar and the working group of which he was the leader (Klobuchar and Working Group, 1979) at the Solar-Terrestrial Predictions Workshop Program in Boulder in 1979. It was concluded that monthly median values of TEC could be predicted to within an rms deviation of 20 to 25 percent in the daytime and 30 to 35 percent at night but that geomagnetic activity causes about a 25 percent deviation from the median values. For highest accuracy in TEC, real-time or near-real-time data are needed. A service is available for registered SELDADS users that provides hourly TEC values from satellite data. SELDADS is an operational, real-time, solar-terrestial-environment monitoring system. Further information about SELDADS and the TEC data that it can provide can be obtained by writing to the Chief Forecaster, Space Environment Services Center, R432, National Oceanic and Atmospheric Adminstration, 325 Broadway, Boulder, CO 80303.

One means for obtaining real-time data on ionospheric TEC is to measure the Faraday rotation of signals from beacons on satellites. In addition to the ionospheric TEC, the total TEC along path to a satellite or space vehicle may include a contribution from the plasmasphere that is about 15 percent of the ionospheric TEC by day and 50 percent by night (Klobuchar and Working Group, 1979). Measurements of time delay at two frequencies can provide the value of the total TEC along a path. As discussed more fully in Sec. 2.3.1, the total TEC is given in that case by Eq. (2.38) which is repeated below.

$$TEC = \frac{\& c}{40.3}\frac{f_1^2 f_2^2}{f_1^2 - f_2^2}$$

The quantities f_1 and f_2 are the two frequencies, c is the velocity of light, and δt is the difference in the time delays (At_2 - At_1) at the two frequencies.

Example 9.2 Effects Dependent on TEC

To illustrate the effects of the total electron content (TEC), frequencies of 870 MHz and 2.3 GHz, a TEC value of i 018 el/m², and a longitudinal component of the Earth's magnetic field B_L of 0.38 B will be utilized.

1. Faraday Rotation

870 MHz, 10^{18} el/m², 0.38 G = 3.8 x 10^{-5} Wb/m²

$$\phi = \frac{2.36 \times 10^4 B_L (TEC)}{f} = \frac{2.36 \times 10^4 (3.8 \times 10^{-5})(10^{18})}{(8{,}7 \times 10^8)^2}$$

$$= 1.17 \text{ rad} = 67.6^\circ$$

2.3 GHz, 10^{18} el/m², 3.8 x 10-S Wb/m²

$$\phi = \left(\frac{8.7 \times 10^8}{2.3 \times 10^9} \right)^2 67.6^\circ = 9.67^\circ$$

2. Time and Range Delay (one-way transmission)

870 MHz, 10^{18} el/m²

$$AR = \frac{40.3 (TEC)}{f^2} \quad \frac{40.3 (10^{18})}{f^2} = 53.24 \text{ m}$$

$$At = \frac{53.24}{2.9979 \times 10^8} = 1.78 \times 10^{-7} \text{ s} = 0.178 \ \mu\text{s}$$

2.3 GHz, 10^{18} el/m²

$$AR = (8.7 \times 108/2.3 \times 10^9)^2 (53.24) = 7.62 \text{ m}$$

$$\Delta t = \frac{7.62}{2.9979 \times 10^{8}} = 0.0254\ \mu s$$

3. Phase Advance (one-way transmission)

870 MHz, 10^{18} el/m^2

$$\Delta\phi = \frac{8.44 \times 10^{-7}}{f}(TEC) \qquad \frac{8.44 \times 10^{-7}\ (10^{18})}{8.7 \times 10^{8}}$$

$= 970.1$ rad or $970.1/2\pi = 154.4$ cycles

This very large advance in phase is of less interest than that due to a change, Δ(TEC), in TEC. Suppose that a traveling ionospheric disturbance modulates TEC by a factor of 0.01 so that $\Delta(TEC) = 10^{16}$ el/m^2. Then

$$\delta\phi \qquad \frac{8.44 \times 10^{-7}}{f}\Delta(TEC) \qquad 9.70 \text{ rad} = 1.54 \text{ cycles} = 556°$$

This still a very large change in phase.

2.3 GHz, 10^{18} el/m^2

$$\Delta\phi = \frac{8.7 \times 10^{8}}{2.3 \times 10^{9}}(9.70) \qquad 367 \text{ rad} = 54.4 \text{ cycles}$$

For modulation of TEC by a factor of 0.01

$\delta\phi = 3.67$ rad $= 0.584$ cycles $= 210$ deg.

4. Doppler Frequency

870 MHz, $\Delta(TEC) = 10^{16}$ el/m^2 in 100 s

$$f_{D} = \frac{1.34 \times 10^{-7}}{f}\frac{\Delta(TEC)}{T_c} = \frac{1.34 \times 10^{-7}(10^{16})}{8.7 \times 10^{8}(100)}$$

$= 0.015$ Hz

2.3 GHz, Δ(TEC) = 10^{16} el/m^2 in 100 S

$$D = \frac{8.7 \times 10^{8}}{2.3 \times 10^{9}} (0.015) = 0.0057 \text{ Hz}$$

5. Dispersion

870 MHz, TEC = 10^{18} el/m^2, Af = 50 MHz

This example applies to the propagation of 2.0 x 10-2 μs pulses through the ionosphere, assuming a system bandwidth Af of 50 MHz with Af = $1/\tau$ where τ is pulse width.

$$|\Delta t| = \frac{2.68 \times 10^{-7}}{f^3} \text{ Af (TEC)} = \frac{2.68 \times 10^{-7} (5 \times 10^{7}) 10^{18}}{(8.7 \times 10^{8})^3}$$

$$|\Delta t| = 2.2 \text{ x } 10\text{-}8\text{s} = 2.2 \times 10^{-2} \mu\text{s} = 22 \text{ ns}$$

The time dispersion is seen to be slightly greater than the pulse width. Thus the dispersion may limit the bit rate (data rate for digital transmission) to something less than 50 Mbps.

2.3 GHz, TEC = 10^{18} el/m^2, Af = 50 MHz

$$|\Delta t| = \frac{8.7 \times 10^{8}}{[2.3 \times 10^{9}]^3} (2.2 \times 10^{-2}) = 1.19 \times 10^{-3} \mu\text{s} = 1.19 \text{ ns}$$

A data rate of 50 Mbps appears to be quite feasible at a frequency of 2.3 GHz.

6. Elevation Angle Error, $\Delta\theta$

870 MHz, 10*^{8} el/m^2

$$\Delta\theta = \frac{\cos \theta_o}{2 h_i} A R$$

In part 2, a range delay AR of 53.24 m was determined for this frequency and TEC. Assuming 400 km for hi and arbitrarily taking θ_o to be 5 deg,

$$\Delta\theta = \frac{0.996}{2\,(4 \times 10^5)} \quad (53.24)$$

$$= 6.6 \times 10^{-5} \text{ rad} = 0.066 \text{ mrad}$$

2.3 GHz, 10^{18} el/m^2

$$\Delta\theta = \frac{0.996}{2\,(4 \times 10^5)} \quad (7.62)$$

$$= 0.0095 \text{ mrad}$$

9.2.3 Ionospheric Scintillation

Scintillation is most severe in the equatorial region within ± 20 deg of the magnetic equator and at high latitudes, where two regions of peak scintillation activity have been reported. One corresponds to the auroral oval, and one is over the polar cap above 80 deg of geomagnetic latitude. In the equatorial zone, scintillation is higher in the region of the equatorial anomaly from about 15 deg to 20 deg north and south of the magnetic equator than near the equator itself. Between the equatorial and high-latitude regions are the middle latitudes where activity is less intense. In all sectors pronounced nighttime maxima occur. The general pattern is as shown in Fig. 9.4. A review of the global morphology of ionospheric scintillation has been provided by Aarons (1982). Some data concerning scintillation levels are shown in Table 9.2 for the low frequencies of 137 and 254 MHz for which scintillation tends to be intense. At Ascension Island in the equatorial anomaly, 27 dB peak-to-peak fading was recorded at 1.54 GHz compared to 7 to 9 dB at Huancayo and Natal near the magnetic equator during the sunspot peak in 1979 and 1980 (Aarons et al., 1981). Further information about scintillation in the equatorial anomaly has been provided by Mullen et al. (1985).

Significant scintillation has been recorded in even the 4 and 6 GHz bands at equatorial latitudes. In one case involving transmission on a 6 GHz uplink and a 4 GHz downlink, fading reached 8 dB peak-to-peak (Aarons, 1982). Examples of scintillation fading on 6 GHz links are shown in Fig. 2.16.

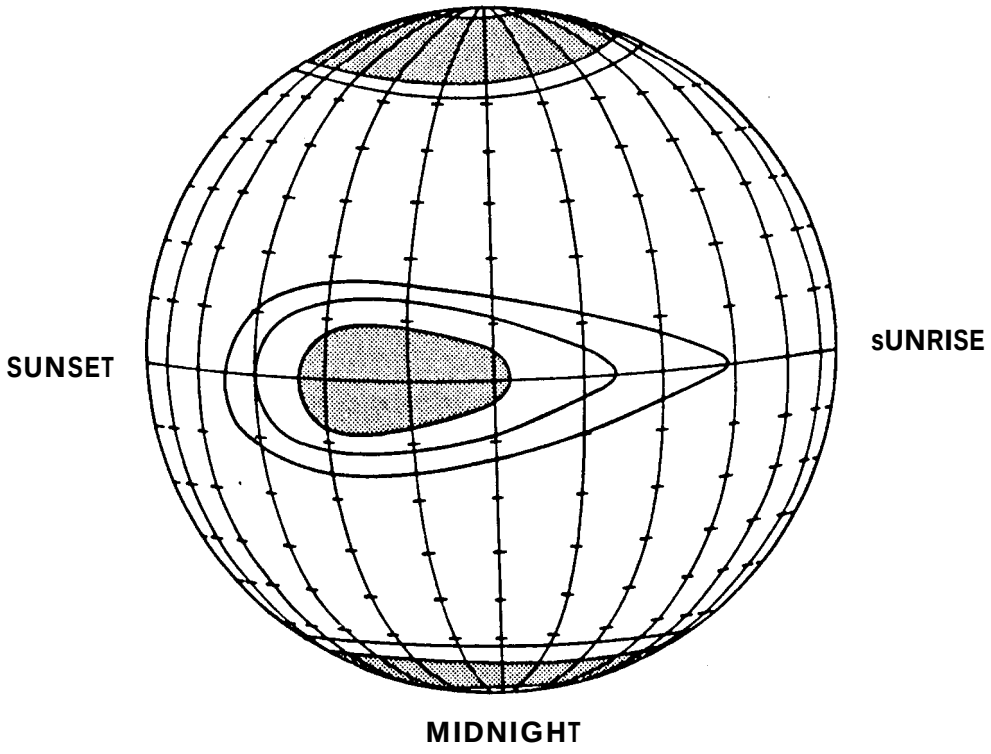

Figure 9.4. Pattern of occurrence of ionospheric scintillation (CCIR, 1986a). -

Although scintillation at middle latitudes is generally not as intense as at equatorial and high latitudes, some cases of severe scintillation have been recorded. During a magnetic storm on March 22.1979, peak-to-peak scintillation of 18, 10, 15, and 3.5 dB were recorded at 136 MHz and 1.7, 4, and 12 GHz, respectively, on different paths in and around Japan (Minakoshi et al., 1981). Also Karasawa et al. (1985) observed fluctuations sometimes exceeding 30 dB peak-to-peak on signals passing over the Indian Ocean at an elevation angle of 17.3 deg.

Considerable data have been accumulated on ionospheric scintillation, and the values quoted here give a rough idea of what margins may be needed to protect against ionospheric stint illation. Table 9.3 gives values of fade depths at midlatitudes (CCIR, 1986a). The data have commonly been presented as peak-to-peak values, and in the case of the 8 dB figure mentioned for 6 GHz-4GHz links not

Table 9.2 Percentage of occurrence of scintillation (CCIR, 1982, 1986a). (a) ≥ 10 dB peak to peak, equatorial latitudes

Location	Frequency	Day	Night
		(400-1600 LT)	(1600-400 LT)
Huancayo, Peru	137 MHz	3	14
	254 MHz	2	7
		(600-1800 LT)	(1800-600 LT)
Accra, Ghana	137 MHz	0.4	14

(b) ≥ 12 dB peak to peak at 137 MHz, subauroral and auroral lat.

Location	K_p	Day (500-1700 LT)	Night (1700-500 LT)
Sagamore Hill, MA	O to 3+	o	1.4
	> 3+	0.1	2
Goose Bay, Labrador	O to 3+	0.1	1.8
	> 3+	1.6	6.8
Narssarssuaq, Greenl.	O to 3+	2.9	18
		19	45

(c) ≥ 10 dB peak to peak at 254 MHz, auroral latitudes

Location	K_p	Day (600-1800 LT)	Night (1800-600 LT)
Goose Bay, Labrador	O to 3+	0.1	0.1
	> 3+	0.3	1.2
Narssarssuaq, Greenl.	O to 3+	0.1	0.9
		2.6	8.4

LT: Local Time

much more than half of the the 8 dB range appeared to involve a signal decrease. The needed margin may thus well be less than the peak-to-peak value. The increase in signal level, however, may in some cases present a problem of overload in itself.

A WBMOD empirical computer model of global scintillation has been prepared by Fremouw and co-workers over a period of years. This model has been described in the review paper by Aarons (1982) and in more detail by Fremouw (1982). Persons wishing to pursue the application of this model to the estimation of ionospheric scintillation may contact Dr. Edward J. Fremouw, Physical Dynamics, Inc., P.0. Box 3027, Bellevue, Washington 98009. A program employing ten frequencies between 137 and 2891 MHz for recording scintillation at equatorial and auroral latitudes was described by Fremouw et al. (1978), and early results of the HiLat mission for obtaining data on the spatial and temporal variation of amplitude and phase scintillation at high latitudes have also been described by Fremouw et al. (1985).

Table 9.3 Distribution of Mid-Latitude Fade Depths in dB due to Ionospheric Scintillation (CCIR, i 982).

Percent of Time Exceeded	Frequency (MHz) 100	200	500	1000
1.0	15.9	1.5	0.2	0.1
0.5	9.3	2.3	0.4	0.1
0.2	16.6	4.2	0.7	0.2
0. i	25.0	6.2	1.0	0.3

9.3 TROPOSPHERIC CLEAR-AIR EFFECTS

9.3.1 Introduction

Clear-air effects on propagation are influenced strongly by the elevation angle of the path. For elevation angles above about 10 deg and for frequencies below about 10 GHz, the effects on communication satellite operations tend to be slight. For elevation angles of only a few degrees, the effects may be severe. The low-elevation-angle effects have long been familiar to persons concerned with terrestrial line-of-sight paths, for which margins up to about 45 dB may be utilized to combat atmospheric multipath fading. For downlinks from satellites, it is difficult to supply large margins and it has been generally assumed that it would not be necessary to do so because large elevation angles would normally be utilized for satellite communications. It turns out, however, that in a number of situations it is desirable to be able to utilize satellites at low elevation angles. The problems of low-angle propagation are well illustrated in a paper on measurements of 1.5 GHz MARISAT signals (Fang, Tseng, and Calvit, 1982). It was reported that MARISAT services were not available for paths having elevation angles below 10 deg because of severe signal degradation. Reflections from the sea surface must have contributed to the problem, but atmospheric effects surely played a major role also,

The time delay due to the atmosphere may be important for navigation, ranging, and time-transfer purposes. The excess range delay caused by the ionosphere on earth-space transmissions can be determined and taken into account by transmitting two different frequencies but that technique cannot be applied to the troposphere as the tropospheric index of refraction does not vary with frequency at radio frequencies.

9.3.2 Refraction and Multipath Fading

The variation of the index of refraction of the troposphere with height causes ray paths to experience bending, which results in errors in measurements of elevation angle. For paths extending to maximum heights of 80 km, as in Table 9.4, the values of elevation angle error are different from the bending values. The amount of bending can be calculated on the basis of an assumed or known index of refraction profile, and then elevation angle error can be calculated. For a much longer path to a geostationary satellite,

Table 9 4 Ray Parameters for a Standard Atmosphere[a,b] (Crane 1976).

Initial Elev. Angle (deg)	Height (km)	Range (km)	Bending (mdeg)	Elev.-Angle Error (mdeg)	Range Error (m)
0.0	0.1	41.2	97.2	48.5	12.63
	1.0	131.1	297.9	152.8	38.79
	5.0	289 3	551.2	310.1	74.17
	25.0	623 2	719.5	498.4	101.0
	80.0	1081.1	725.4	594.2	103.8
5.0	0.1	1.1	2.6	1.3	0.34
	2.0	11.4	25.1	12.9	3.28
	5.0	55.2	91.7	52.4	12 51
	25.0	241.1	176.7	126.3	24 41
	80,0	609.0	181.0	159.0	24 96
50.0	0.1	0.1	0.2	0.1	0 04
	1.0	1.3	1.9	1.0	0 38
	5.0	6.5	7.0	4.0	1 47
	25.0	32.6	14.3	10.3	3.05
	80.0	104.0	14.8	13.4	3.13

[a]U.S. Standard Atmosphere Supplements. 1966. Environmental Sci. Serv. Administration, Dept. of Commerce, Washington, DC (1966).

[b]Sissenwine, N., D.D. Grantham, and H.A. Salmela, AFCRL-68-0556, Air Force Cambridge Res. Lab., Bedford, MA (Oct. 1968),

Table 9.5 Ray Bending Values (CCIR, 1986b).

Elevation angle	Average bending	
	Polar continental	Tropical maritime
1°	0.45°	0.65°
2°	0.32°	0.47°
4°	0.21°	0.27°
10°	0.1O°	0.14°

however, one can calculate values for bending, such as those displayed in Table 9.5, and take the corresponding elevation-angle error values to be the same as the bending values, no further calculation being needed.

Atmospheric multipath fading is a serious problem for very-low-elevation-angle paths, whether terrestrial or earth-space. The amount of fading is best determined by experimental data for the particular path, and the margin to be utilized for fading depends on the grade of service needed. An effort is made here to distinguish between refractive multipath fading and tropospheric scintillation, but the distinction is not always made clearly in the literature nor is it always possible to distinguish the two phenomena in practice. Atmospheric multipath fading is generally restricted to angles less than 10 deg and is most serious for angles up to only a few degrees. It is considered to result from large-scale changes in refractivity and involves relatively long fading periods, generally from about 10 s to a few minutes. Scintillation results from the smaller-scale structure of turbulence and clouds and has short periods in the order of a second and less. Though most intense for low elevation angles, it does not decrease as rapidly with increasing elevation angle as multipath fading. Tropospheric multipath fading tends to be insensitive to frequency over the microwave frequency range. It is often associated with the occurrence of temperature inversions and disappears when the temperature inversion is destroyed by the passage of cyclonic storms (Flock, 1960).

Although sometimes referred to as scintillation, the fading observed at 4 and 6 GHz in the Canadian Arctic at an elevation angle of one deg (Strickland et al., 1977) is undoubtedly atmospheric multipath fading. The margins judged to be required for such operation for three values of reliability or availability are shown in Table 9.6. The refractivity y in the Arctic tends to be less than in other sections of the world, perhaps excluding desert areas, and similar or higher margins would probably be required elsewhere for the same elevation angle. On a path in Hawaii at the slightly larger elevation angle of 2.5 deg, Thompson et al. (1975) observed fading of 20 dB.

Table 9.6 Six GHz Link Margins in dB for Tropospheric Fading at Eureka, Ellesmere Island, Canada, Elevation Angle One Degree (Strickland et al., i 977).

Time Duration	Reliability (percent)		
	90	99	99.9
Worst two hours	8.0	18.0	28.0
Worst summer day	6.8	15.5	24.5
Worst summer week	5.4	13.0	22.0
Worst month, July	3.8	10.8	20.3

9.3.3 Tropospheric Scintillation

The term tropospheric scintillation is used here to refer to generally low-amplitude, rapid variations in signal intensity with periods typically around one second. Such scintillation tends to be associated with small-scale structure such as that of turbulence and clouds. The amplitude variance due to scintillation has been modeled as a function of frequency and elevation angle (Ippolito, Kaul, and Wallace, 1983). The results of this analysis show that scintilla ion amplitude increases with frequency and decreases with elevation angle (Fig. 9.5).

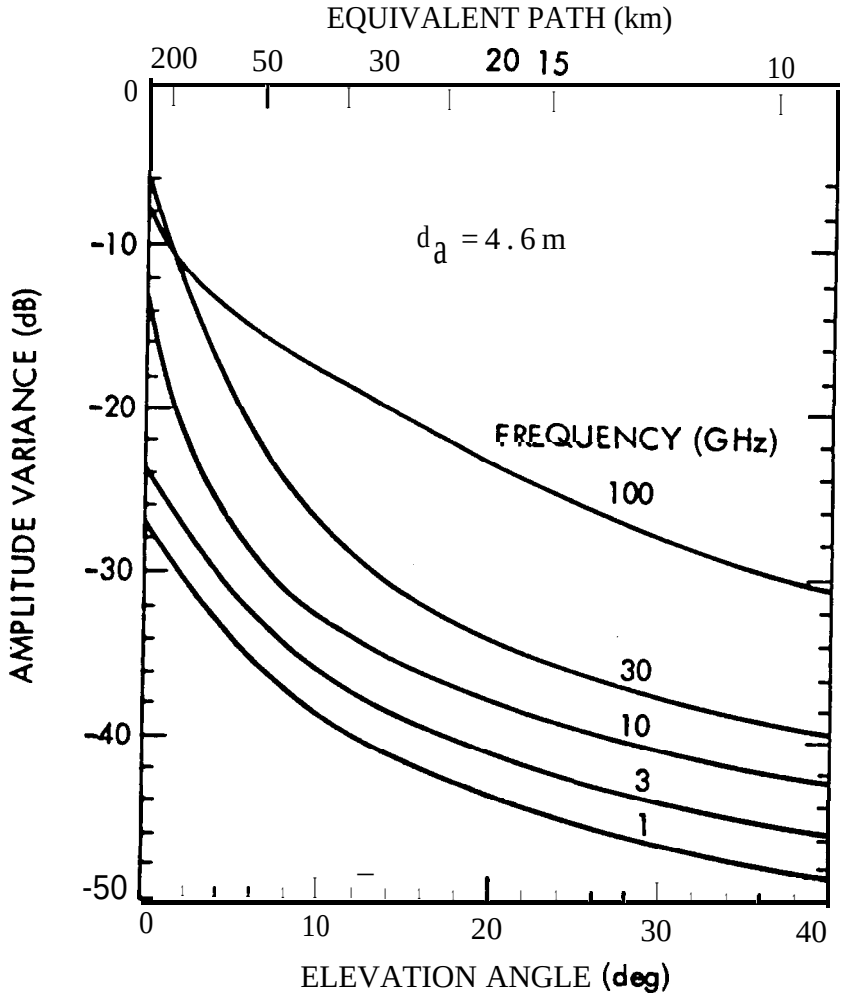

Figure 9.5. Amplitude variance for a 4.6 m diameter aperture for 1 to 100 GHz (Ippolito, Kaul, and Wallace, 1983).

Example 9.3 Tropospheric Refraction

Tropospheric refraction may result in elevation-angle error, ducting, and/or multipath fading. The material of this Sec. 9.3 and Chap. 3 include illustrative 'values of elevation-angle error and multipath fading, but it is difficult to compose suitable quantitative numerical calculations relating to these effects. All are functions of the index of refraction profile. Calculation of refractivity N is illustrated in this example.'

The refractivity of the troposphere is described by the following relation [Eq. (3.2)].

$$N = \frac{77.6\ p}{T} + \frac{3.73 \times 10^5\ e}{T^2}$$

where N = (n - 1) x 10^6 with n the index of refraction, p the total pressure in mb, e the partial pressure of water vapor in mb, and T the temperature in k elvins. " Values of N that" would apply to Denver, Colorado for the pressure of a standard atmosphere and a surface temperature of 20 deg C will now be calculated for water vapor specified in two ways. First a water vapor density of 7.5 g/m^3 is assumed, and secondly a relative humidity of 60 percent is assumed.

For the U.S. Standard Atmosphere, the pressure p at an altitude of 1600 m (1 mile) is 835 mb, compared to 1013 mb at sea level. The temperature of 20 deg C corresponds to a temperature in kelvins of 273 + 20 = 293 K.

1. Water vapor density $\rho = 7.5\ g/m^3$

Using Eq. (3.5), $e = \frac{\rho T}{216.5} \quad \frac{(7.5)\ (293)}{216.5} = 10.15$ mb

$$N = \frac{77.6\ (835)}{293} + \frac{3.73 \times 10^5\ (10.15)}{(293)^2} = 222.1 + 44.1$$

$$N = 265.2$$

2. Relative humidity (R. H.) 60 percent

From Table 3.1 for T 20° C, e_s, the saturation water vapor pressure equals 23.4 mb.

e = es (R. H.) = (23.4) (0.60) = 14.04 mb

$$N \quad \frac{77.6\ (835)}{293} + \frac{3073 \times 10^5\ (14.04)}{(293)^2} = 222.1 + 61.0$$

N 282.1

The above values of N are rather low because of the reduced pressure at the altitude of Denver. For the same water vapor contents of 7.5 g/m^3 and 60 percent relative humidity at 20 deg C but the sea level pressure of 1013 mb, the corresponding values of N are 313.5 and 330.5 respectively. To illustrate what is probably the maximum value of N that might be encountered consider the temperature of 34 deg C and a partial pressure of water vapor of 53.2 mb, values recorded at Sharjah, Saudi Arabia. For this case

$$N = \frac{77.6\ (1013)}{307} + \frac{3.73 \times 10^5 (53.2)}{(307)^2} = 256.1 + 210.5$$

$$N = 466.6$$

It is the variation of N with height that has the greatest effect on wave propagation, a decrease of 157 N/km being sufficient to cause trapping or ducting of a wave launched at an elevation angle of zero degrees. Still higher rates of decrease can trap waves having elevation angles slightly greater than zero degrees. An expression provided by Bean and Dutton (1966), namely

$$\frac{\Delta n}{\Delta r} = - \left[\frac{1}{r_0} + \frac{(32}{2 h_a} \right.$$

allows determining that for a decrease of 300 N/km ($\Delta n/\Delta r$ = -().000300) in a layer of thickness h_a of 0.1 km at the Earth's surface, taking r. as 6370 km,

$$\theta_p = 5.3 \text{ mrad} = 0.3 \text{ deg}$$

The angle 6_p is the penetration angle. Rays having smaller values are subject to ducting.

9.3.4 Defocusing

Bending of rays is proportional to dN/dh, the variation of refractivity y N with height (Sec. 3.2), and when dN/dh itself varies with height rays at different heights experience different amounts of bending. As a result the rays become more widely separated

than previously and signal intensity is reduced. Figure 8.5 shows the attenuation due to defocusing as a function of elevation angle and AN, the decrease in refractivity in the first km above the surface. Figure 9.6 shows the defocusing loss in a different way. Here the loss corres onding to the average of many index of refraction profiles aJ the standard deviation of the loss are shown as a function of elevation angle. The results were obtained at Albany, New York and are representative of an inland continental location.

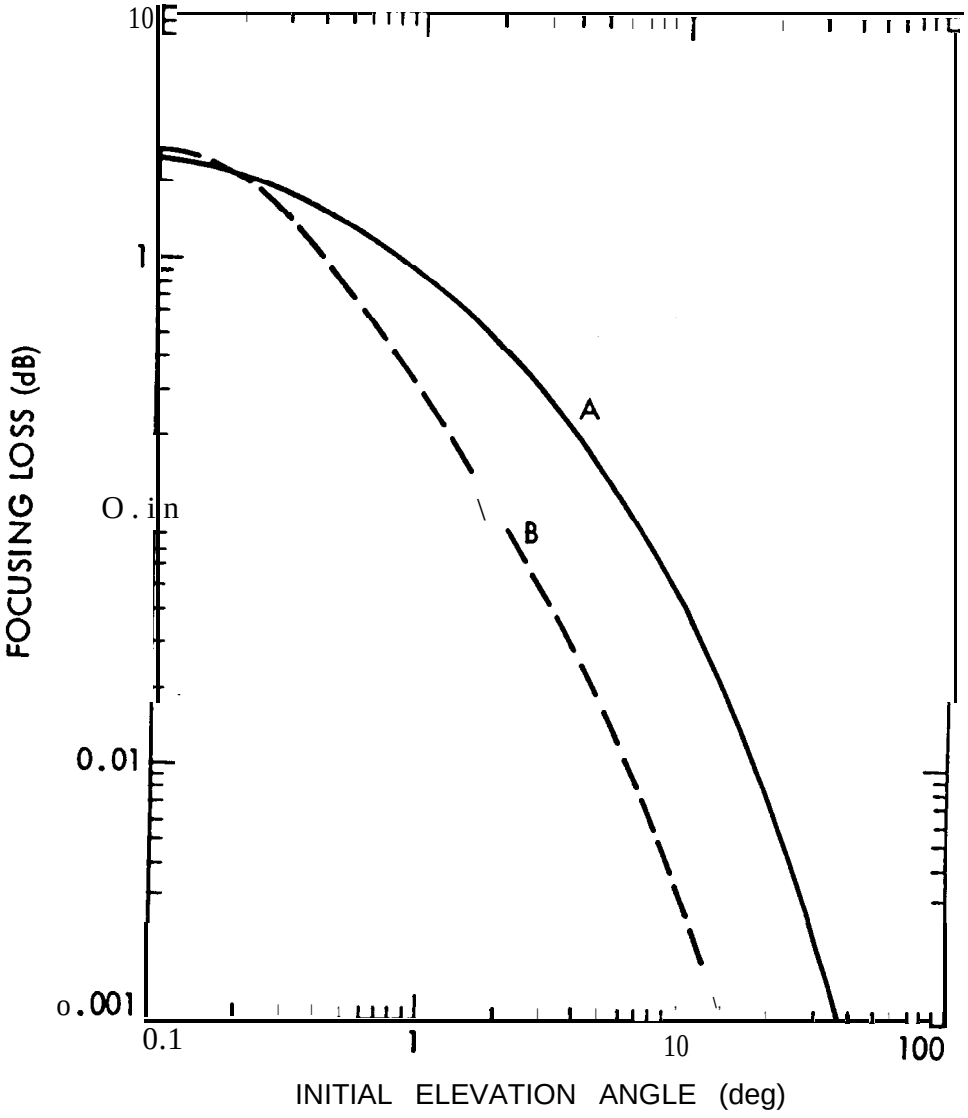

Figure 9.6, Average focusing loss (A) and standard deviation about the average (B) (CCIR, 1986b).

9.3.5 Gaseous Attenuation

The attenuation constants for oxygen and water vapor are shown in Fig. 3.10 for sea-level pressure, a temperature of 15 deg C, and a water vapor density of 7.5 g/m^3. At 10 GHz, the attenuation for oxygen is about 0.007 dB/km, and it decreases only slowly to about 0.005 dB/km at 1 GHz. For water vapor the value is only about 0.006 dB/km at 10 GHz, and the attenuation drops rapidly below 10 GHz. The total vertical one-way attenuation due to the gaseous constituents of the atmosphere from sea level to the top of the atmosphere for a water vapor density of 7.5 g/m^3 is shown in Fig, 3.11. For 10 GHz the value is nearly 0.06 dB For 10 GHz and a height of 4 km, CCIR Report 719 for 1978 showed a value slightly over 0.02 dB for the total zenith attenuation.

In treatments of coordination distance, as in Chap. 8, it is usually considered that attenuation due to water vapor can be neglected below 10 GHz but that attenuation due to oxygen should be included. For coordination distance analysis, the recommended values of water vapor density range from 1 to 5 g/m^3. Use of these lower densities is conservative when considering interference and gives lower attenuation, of course, than for 7.5 g/m^3.

Analytical expressions for the attenuation constants due to oxygen and water vapor are also given in Chap. 3 [Eqs. (3.20) and (3.21)], and expressions are also given for the total attenuation [Eqs. (3.22) and (3.23)]. Nonlinear effects that complicate the analysis for water vapor densities of 12 g/m^3 and higher are presently being studied.

9.3.6 Excess Time and Range Delay

The excess time and range delays for propagation of signals through the Earth's atmosphere consist of components caused by the ionosphere and by the troposphere. The delay due to the ionosphere was considered in Sec. 9.2.2. Time delay Δt and range delay AR are related by $AR = c\ \Delta t$, where c is the velocity of light in a vacuum, about 2.9979 x 108 m/s, The discussion in this section is in terms of AR.

The excess tropospheric range delay can be separated into the delay due to dry air AR_d and the delay due to water vapor AR_w or, somewhat more conveniently, it can be separated into AR_1 and ΔR_2

corresponding to the two terms of the expression for the refractivity of the troposphere (Sec. 3.7; Flock, Slobin, and Smith, 1982). The equation for N is

$$N = \frac{77.6\ p}{T} + \frac{3.73 \times 10^5\ e}{T^2} \qquad (9.18)$$

The range delay ΔR_1 for a vertical path due to the first term of Eq. (9.18) is given by

$$\Delta R_1 = 10^{-6} \int N_1\ dh = 10^{-6} \int \frac{77.6\ p}{T}\ dh = 2.757 \times 10^{-3}\ p_0\ m \qquad (9.19)$$

for a latitude of about 45° (only slightly different elsewhere) where p. is total surface pressure in mb. For p_0 = 1013 mb, the approximate value for sea level, AR_1 = 2.31 m. The total pressure $p = p_d + e$ where p_d is the pressure of dry air and e is the partial pressure of water vapor. As pd is much larger than e, AR_1 is largely but not entirely due to dry air. Hopfield (1971) has determined that ΔR_1 can be determined to an accuracy of 0.2 percent or about 0.5 cm by measuring p_o.

It is shown in Sec. 3.7 that ΔR_2 for a vertical path is given by

$$\Delta R_2 = 10^{-6} \int N_2\ dh = 1.731 \times 10^{-3} \int \frac{P}{T}\ dh \qquad (9.20)$$

where p is the density of water vapor in g/m^3. Water vapor density p in g/m^3 and water vapor pressure e in mb are related by p = (e 216.5)/T where T is in kelvins as in Eq. (9. 18). Determining a value for AR_2 requires information on ρ and T as a function of height. As p is highly variable and difficult to predict from surface parameters, water vapor is responsible for a larger error in range than is dry air even through the magnitude of AR_2 is typically only about 10 cm for ρ = 7.5 g/m^3 at the surface. By the use of radiometer techniques, however, AR_2 can be determined to an accuracy of possibly 0.5 cm (Sec. 3.7).

Table 9.4 includes values of total excess tropospheric range delay for paths to 80 km at several different elevation angles.

Example 9.4 Tropospheric range delay

To illustrate the magnitude of excess range delay due to the troposphere, consider first a zenith path at Denver , Colorado where the surface pressure for a standard atmosphere is 835 mb. From Eq. (9. 19) the typical delay corresponding to the first term of the expression for N is

$$\Delta R_1 = 2.2757 \times 10^{-3} p_0 = 1.90 \text{ m}$$

A more reliable value at a particular time could be obtained by using the measured value of p. at that time rather than the value for a standard atmosphere. For a relative humidity of 60 percent and other conditions likewise as in Example 9.3, the delay corresponding to the second term of the expression for N could be obtained approximately by first calculating the value of N_2 by use of

$$N_2 = \frac{3.73 \times 10^5 (14.04)}{(293)^2} = 61.00$$

Then assuming an exponential decrease of N_2 with a scale height of 2 km

$$\Delta R_2 = 10^{-6} \int 61.00 \, e^{-h/2000} \, dh = 10^{-6} (61.00) (2000)$$

$$\Delta R_2 = 12.2 \text{ cm}$$

The total excess delay AR for a zenith path would then be

$$AR = \Delta R_1 + AR_2 = 2.02 \text{ m}$$

For a path at an elevation angle of 30 deg the corresponding delay would be 2.02/sin 30 deg = 4.04 m. The calculation of AR_2 is illustrative only, and the most accurate determination of AR_2 requires information about the actual value of N_2 as a function of height above the surface or the use of radiometer techniques (Sec. 3.7).

9.4 ATTENUATION AND DEPOLARIZATION CAUSED BY PRECIPITATION

9.4.1 Introduction

Attenuation caused by rain increases with frequency throughout the microwave range and has sometimes been considered to be important only for frequencies above 1 O GHz. However, while it is true that attenuation decreases rapidly with decreasing frequency below 10 GHz, values of attenuation are nevertheless potentially troublesome for frequencies of 8 GHz or lower, In addition the attenuation due to rain is accompanied by an increase in antenna noise temperature which further degrades the carrier power-to-noise ratio (See.9.7).

Depolarization due to rain is caused by differences in attenuation and phase shift of electric-field-intensity components that are parallel to the major and minor axes of rain drops, which are roughly spheroidal in form. The most favorable condition for these differences to be high is for the absolute values to be high. Thus depolarization tends to be most severe when attenuation is high, and it might be expected that as attenuationis low for frequencies below 8 GHz depolarization would also be low. Attenuation at 4 GHz, for example, is only about 0.05 dB/km for a rain rate of 35 mm/h, Depolarization does tend to decrease with decreasing frequency, but it does so less rapidly than attenuation because differential phase shift as well as differential attenuation contributes to depolarization, and differential phase shift is relatively high for frequencies below 10 GHz. (Phase shift is proportional to the real part of the effective index of refraction of a medium, and this value is relatively high below 10 GHz as shown in Fig, 4.3.) It thus develops that depolarization due to rain may be important for frequencies of 4 GHz or lower.

Scatter of electromagnetic waves by rain is significant for frequencies of 1,5 GHz or lower, as the intense echoes from rain on L-band radar displays indicate. Such scatter in a potential source of interference (Chap. 8).

Basic concepts and definitions concerning the propagation effects of rain were presented in Chap. 4. Consideration is directed here to procedures for estimating the magnitude of the effects and to numerical examples.

9.4.2 Estimation of Attenuation Due to Rain: Step-by-step Procedure.

In the design of telecommunication links, data on propagation effects are needed in statistical form in order to provide as much assurance as possible that a certain signal level will be available for a specified percentage of time. A sufficient data base is not available for all popagation effects to allow link design on this basis, but a consierable effort has been devoted to the development of satisfactory data bases and models to account for the effects of rain in this way.

If satisfactory statistical data on rain rate or attenuation due to rain are available for the particular location in question they should be used. Lin (1977) and Lee (1979) have described procedures for obtaining the needed rain rate statistics from data supplied by the National Climatic Data Center in the United States. Lacking the information needed to proceed on the basis of local weather data or not wishing to formulate statistical data from Weather Service records, use can be made of models that have been developed for rain rate and attenuation due to rain. The steps to be taken in estimating attenuation are listed below. The application of the modified 1982 CCIR model is emphasized. Other models are described in Sec. 4.3.3.

1. Estimate Rain Rate

A first step in obtaining a value of attenuation due to rain is to estimate the rain rate R that is exceeded for the percentage or percentages of time of interest. The small percentage of 0.01 corresponding to 53 minutes per year is commonly the value that is utilized. Even if interest lies in, or includes, other percentages, the modified 1 982 CCIR procedure calls for determining the attenuation for a percentage of 0.01 initially. For estimating R, use should be made of statistical data for the particular location, if satisfactory data are available, or of several models described in Sec. 4.3.3. Prominent among these is the 1980 Global Model by Crane (1980a), Figure 4.8 shows the rain-rate re ions of the world according to this model, and Figs. 4.9 and 9.7 show rain-rate regions of the United States in more detail. The rain-rate values for these regions are given in Table 9.7.

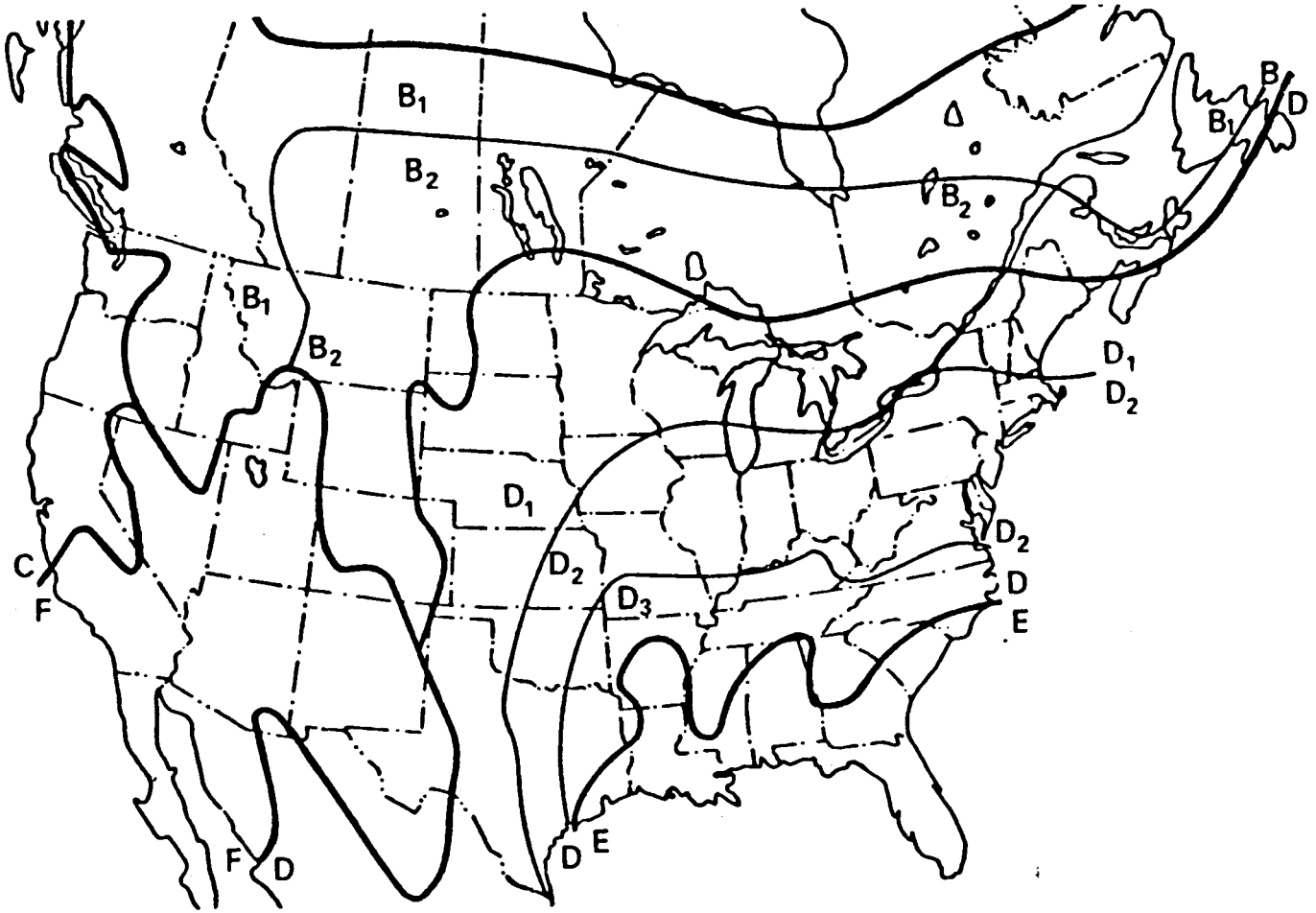

Figure 9.7. Rain-rate regions for conterminous United States and southern Canada (Crane, 1980b).

Table 9.7 Point Rain-Rate Distribution Values (mm/h) Versus Percent of Year Rain Rate is Exceeded (Crane, 1980b).

Percent of Year	RAIN CLIMATE REGION												Minutes per Year	Hours per Year
	A	'1	B	B_2	C	'1	$D=D_2$	'3	E	F	G	H		
0.001	28.5	45	57.5	70	78	90	108	126	165	66	185	253	5.26	0.09
0.002	21	34	44	54	62	72	89	106	144	51	157	120.5	10.5	0.18
0.005	13.5	22	28.5	35	41	50	54.5	30.5	118	34	20.5	178	26.3	0.44
0.01	10.0	15.5	19.5	23.5	28	35.5	49	63	98	23	94	147	52.6	0.88
0.02	7.0	11.0	13.5	16	18	24	35	48	78	15	72	119	105	1.75
0.05	4.0	6.4	8.0	9.5	11	14.5	22	32	52	3.3	47	86.5	263	4.38
0.1	2.5	4.2	5.2	6.1	7.2	9.8	14.5	22	35	5.2	32	64	526	8.77
0.2	1.5	2.8	3.4	4.0	4.8	6.4	9.5	14.5	21	3.1	21.8	43.5	1052	17.5
0.5	0.7	1.5	1.9	2.3	2.7	3.6	5.2	7.8	10.6	1.4	12.2	22.5	2630	43.8
1.0	0.4	1.0	1.3	1.5	1.8	2.2	3.0	4.7	6.0	0.7	8.0	12.0	5260	87.7
2.0	0.1	0.5	0.7	0.8	1.1	1.2	1.5	1.9	2.9	0.2	5.0	5.2	10520	175
5.0	0.0	0.2	0.3	0.3	0.5	0.0	0.0	0.0	0.5	0.0	1.8	1.2	26298	438

The modified 1982 CCIR model uses similar but somewhat different rain-rate regions (CCIR, 1986c). These are shown in Figs. 4.13-4.15, and the corresponding rain-rate values are given in Table 4.5. Figure 4.10 shows the CCIR regions for Canada, as modified by Segal (1986), and we recommend using these for Canada whether otherwise following the CCIR model or not. Contours of rain rate exceeded for 0.0 1 percent of the time according to the modified 1982 CCIR model are reproduced here as Figs. 9.8-9.10. Table 4.5 gives rain rates exceeded for percentages other than 0.01, and attenuations for the other percentages were calculated independently for continental climates in the original 1982 model. The present CCIR procedure, however, is to calculate the attenuation for a percentage of 0.01 and to modify the value determined in this way ifan attenuation for another percentage is desired.

The large-scale world-wide or continent-wide maps of rain-rate regions are extremely valuable but suffer from lack of detail. This statement is especially applicable to the western United States where large variations in rain rate occur within short distances. Rain rates on opposite sides of mountain ranges, for example, are often drastically different. As pointed out in CCIR Report 563-3, (CCIR, i 986c) additional data are needed to improve the accuracy and resolution of the information on rain rates. A considerable amount of data on the effects of rain has been accumulated for the eastern United States and is reflected in Fig. 9.7. For the United States, we recommend using the rain-rate regions of Fig. 9.7 and the values of Table 9.7. For Canada we favor the modified CCIR regions of Fig. 4.10 and the values of Table 4.5. For the rest of the world, we favor the regions and values of the modified 1 982 CCIR model. (Figs. 4.13-4.15 and Table 4.5 or Figs. 9.8-9. 10 for a percentage of occurrence of O.01).

2. Determine Attenuation Constant Corresponding to Rain Rate

For the rain rate R determined in step i, find the corresponding attenuation constant α_p by use of an expression of the form of $\alpha_p = aR^b$. Values of the coefficients of a and b, based on the assumption of s herical drops, have been provided by Olsen, Rogers, and Hedge (19?8), and their values for frequencies of 15 GHz and lower are reproduced as Table 4.2. A trend exists, however, to account for

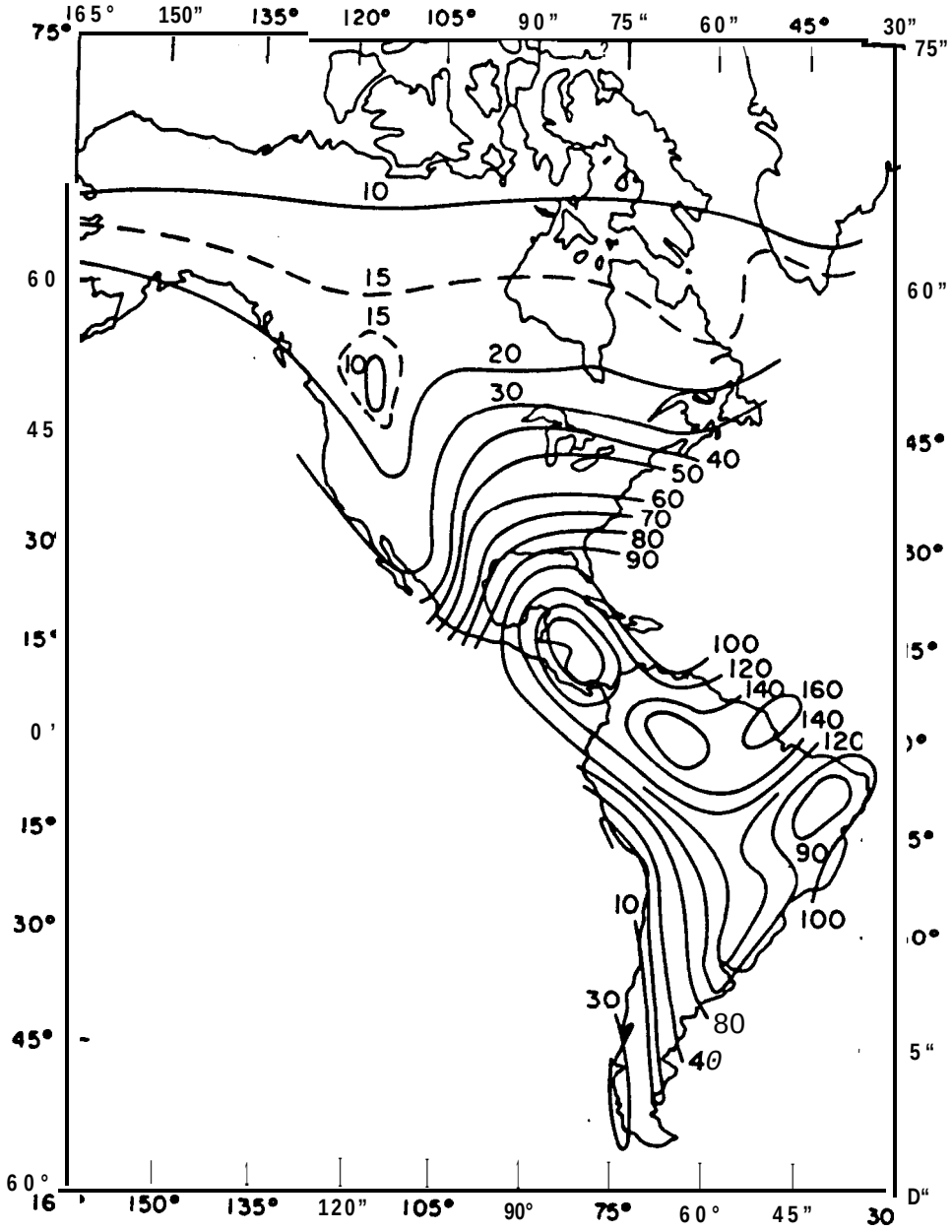

Figure 9.8. Contours of rain rates (mm/h) exceeded for 0.01 percent of the time, the Americas (CCIR, 1986c).

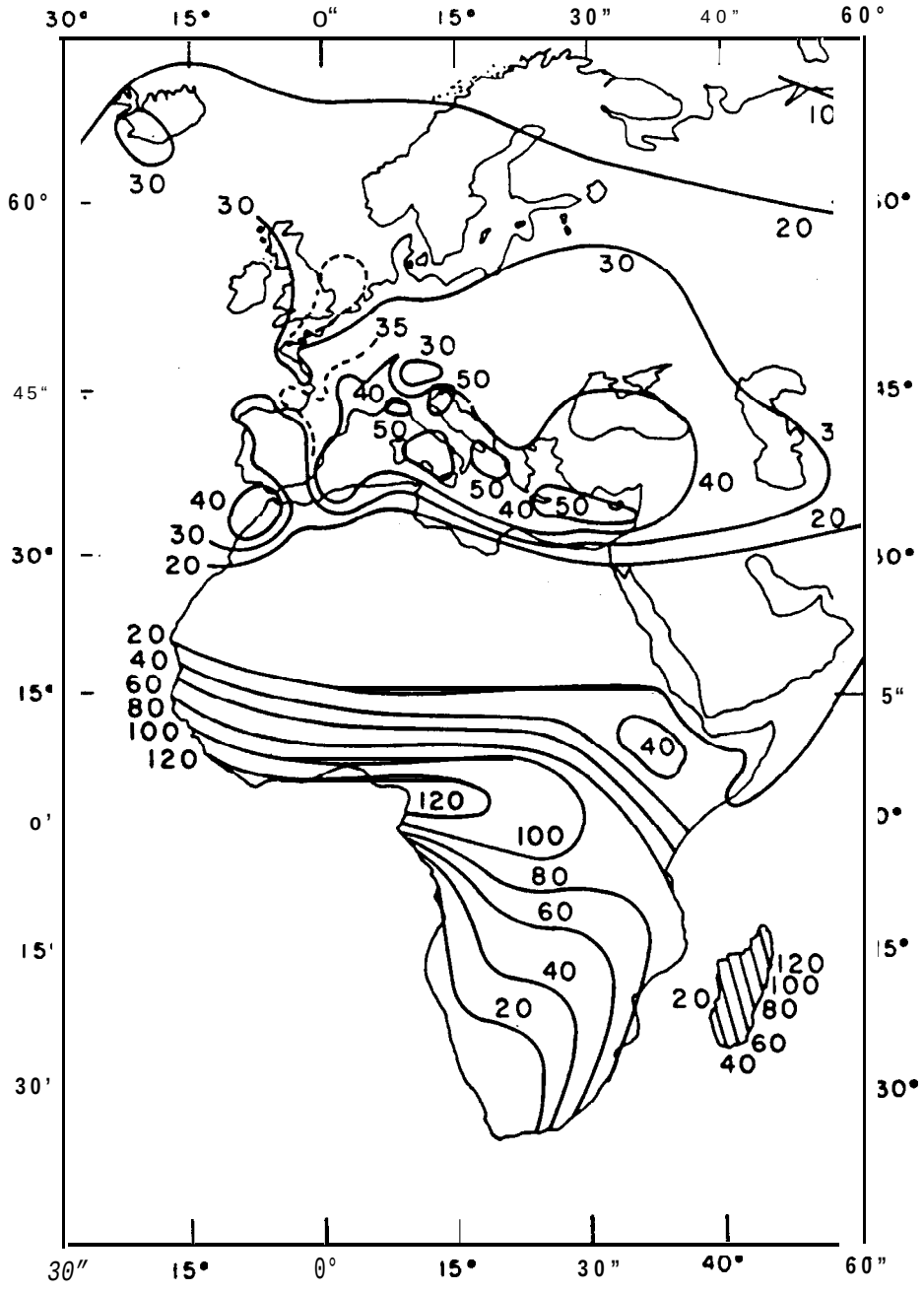

Figure 9.9. Contours of rain rates (mm/h) exceeded for 0.01 percent of the time, Europe and Africa (CCIR, 1986c).

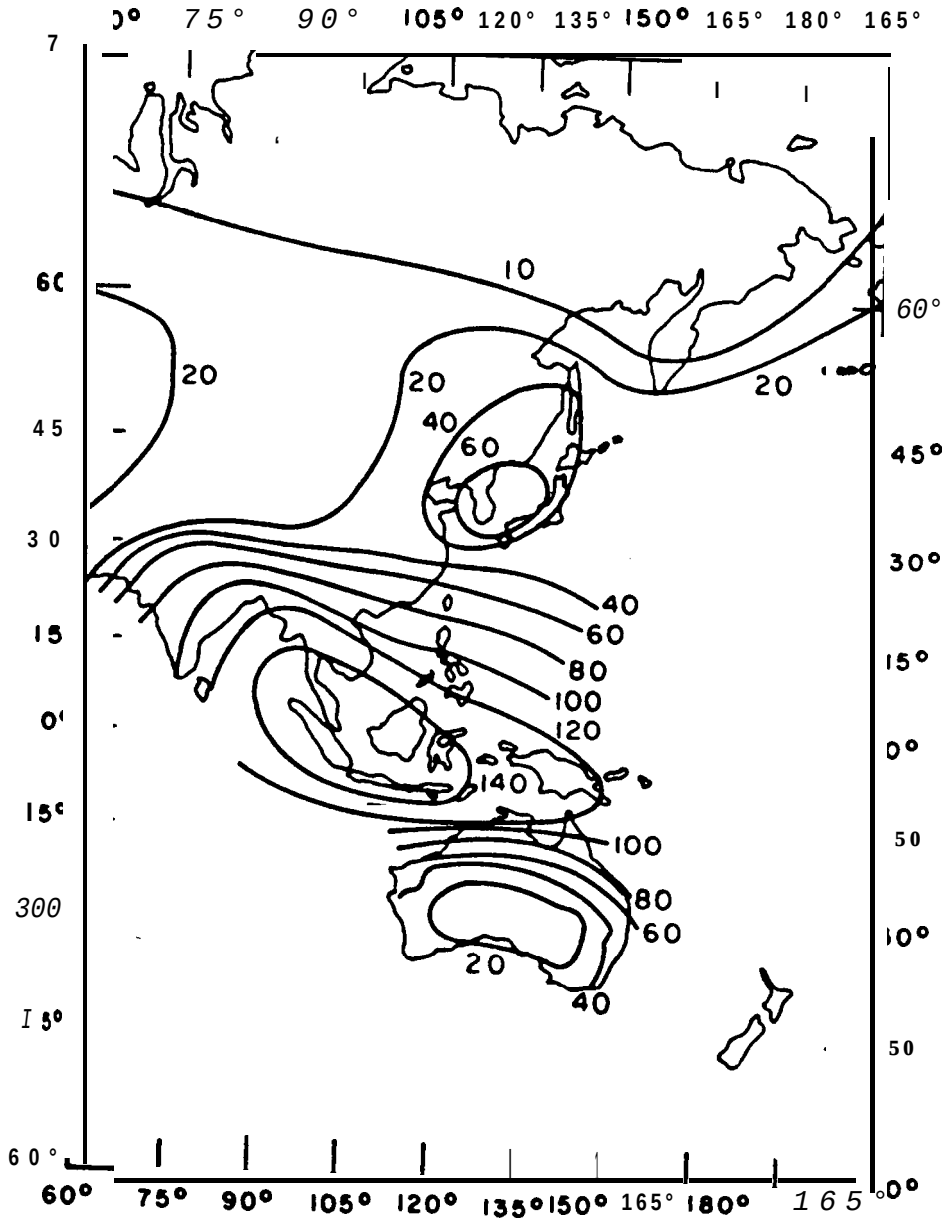

Figure 9.10, Contours of rain rates (mm/h) exceeded for 0.01 percent of the time, Asia and Oceania (CCIR, 1986c).

the non-spherical shape of raindrops and to therefore distinguish between horizontal and vertical linear polarization and circular polarization. Values of a and b for the two linear polarizations are given for a limited number of frequencies in Table 9.8 (CCIR, 1986d). Then for arbitrary linear polarization and for circular polarization values of a and b (a_c and b_c) are given by

$$a_C = [a_h + a_v + (a_h - a_v)\cos^2\theta \cos 2\tau] / 2 \quad (9.21)$$

$$b_C = [a_h b_h + a_v b_v + (a_h b_h - a_v b_v)\cos^2\theta \cos 2\tau] \backslash 2a_c \quad (9.22)$$

where h and v refer to horizontal and vertical polarization, θ is the elevation angle of the path, and τ is the polarization tilt angle of a linearly polarized wave (see Sec. 9.4.3.2). For circular polarization τ can be taken to be 45 deg, and it can be seen that Eqs. (9.2 1) and (9.22) simplify considerably in that case.

Other means are available to obtain values of α_p as a function of frequency and rain rate. Figures 4. 3b and 4.5, for example, can be used for this purpose with α_p given by $(2\pi/\lambda)\, m_i$ if Fig. 4.3b is used. As in some cases these figures provide only an approximate value because of the way they are plotted, they are perhaps best used as a rough check on the values obtained by using $\alpha = aR^b$.

3. Determine Path Length L and Horizontal Projection D

In addition to the attenuation constant, α, in dB/km, information on the path length L through rain is needed to determine total attenuation along the path. Rainis essentially confined to the region below the height of the O deg isotherm. In the previous edition of this handbook, the curves of Fig. 4.7, especially the dotted modification of the curve for the percentage of 0.01 for latitudes below 40 deg, were featured. The latest CCIR procedure, however, is to use Eq. (9.23) for the height extent H of rain for latitudes ϕ of 36 deg or greater and for a time percentage of 0.01 (CCIR, 1986e).

$$H = 4.0 - 0.075\ (\phi - 36^\circ)\ \text{km} \quad (9.23)$$

For latitudes less than 36 deg, H is taken to be 4.0 km.

Table 9.8 The Coefficients a and b for Calculating Attenuation for Horizontal and Vertical Polarization (CCIR, i 986d).

f (GHz)	ah	a_v	b_h	b_v
1	0.0000387	0.0000352	0.912	0.880
2	0.000154	0.000138	0.963	0.923
4	0.000650	0.000591	1.121	1.075
6	0.00175	0.00155	1.308	1.265
8	0.00454	0.00395	1.327	1.310
10	0.0101	0.00887	1.276	1.264
12	0.0188	0.0168	1.217	1.200
15	0.0367	0.0335	1.154	1.128

For elevation angles above 1 O deg, determine the length L of the path through rain by use of

$$L = \frac{H}{\sin \theta} - \frac{H_o - H_g}{\sin e} \quad \text{km} \qquad (9.24)$$

where θ is elevation angle, H_g is the height above sea level of the surface, Ho is the height of the O deg C isotherm, and $H = H_o - H_g$. For elevation angles less than 10 deg, the path length L can be determined from

$$L = \frac{2H}{(\sin^2\theta + \frac{2H}{k r_o})^{1/2} + \sin \theta} \quad \text{km} \qquad (9.25)$$

where kr_o is the effective radius of the Earth (Sec. 3.2) and can be taken to be 8500 km for k = 4/3 in the absence of contrary information. For determining D, the horizontal projection of L, use $D = L \cos \theta$.

4. Path Reduction Factor; Effective Path Length

The average rain rate along a path through rain tends to differ from the rain rate at a particular point. For high values of rain rate at a point, the average rate tends to be less, as intense rain is generally restricted to localized areas. This problem has been approached by determining a path reduction factor which can be viewed as modifying the value of R to obtainan effective value oras modifying L to obtain an effective path length.

Following the modified CCIR procedure (CCIR, 1986e), one determines the path reduction factor r_p for a probability of 0.01 percent from

$$r_P = \frac{1}{1 + 0.045\ D} \tag{9.26}$$

where D is the horizontal projection of the path length L. Previously different coefficients of D were used for rain rates exceeded for different percentages of time, but, as mentioned under step 1, the latest procedure is to make the calculation of attenuation for 0.01 percent and to modify the value so determined to obtain attenuations for other percentages. Also the previous form was 90/ (90 + 4D), but if numerator and denominator of this expression are divided by 90 an expression very close to that of Eq. (9.26) results.

5. Calculate Attenuation

Having determined the values of α_p, L, and r_p for a percentage of 0.01, attenuation A in dB can be calculated, using the modified CCIR model, from the simple relation

$$A = a_P\ L\ r_P \quad \text{dB} \tag{9.27}$$

Attenuations equaled or exceeded for percentages p other than 0.01 percent can be found from the attenuation $A_{0.01}$ for 0.01 percent by use of

$$A_p = A_{0.01}\, 0.12\, p^{-(0.546 + 0.043 \log p)} \qquad (9.28)$$

Previously the recommendation was to use Fig. 4.12 or its algebraic equivalent for the same purpose as Eq. (9.28).

It should be kept in mind that attenuation due to rain is accompanied by an increase in system noise temperature. Thus the degradation in signal-to-noise ratio due to rain is more severe than that caused by attenuation alone, especially for low-noise systems. Section 9.7 and Chap. 7 are devoted to the subject of noise.

Example 9.5 Attenuation Due to Rain

For an example of attenuation caused by rain, we find attenuation values applicable in western Kansas at a latitude of 40 deg at a frequency of 8.5 GHz.

1. Figure 9.7 shows western Kansas to be in region D_1 of the 1980 Global Model, and Table 9.7 shows the rain exceeded for 0.01 percent of the time to be 35.5 mm/h.

2. To determine applicable attenuation constants, use

$$\alpha_p = a(f)\, R^{b(f)}$$

with constants a and b from Table 9.9, using interpolation between values for 8 and 10 GHz. Values of the constants will be determined for horizontal, vertical, and circular polarizations, using Eqs. (9.21) and (9.22) for circular polarization.

The values of a and b for 8.0 GHz and 10.0 GHz and linearly interpolated values for 8.5 GHz are as follows:

f (GHz)	a_h	a_v	b_h	b_v	a_c	b_c
8	0.00454	0.00395	1.33	1.31	–	–
10	0.1010	0.00887	1.28	1.26		
8.5	0.00593	0.00518	1.32	1.30	0.00556	1.31

Use of the a and b entries result in values of α_p in dB/km of 0.660 for horizontal polarization, 0.537 for vertical polarization, and 0.597 for circular polarization.

3. For determining path length L and horizontal projection D use

$$H = 4{,}0\text{-}0.075\ (\phi - 36°)\ \text{km}$$

For $\phi = 40^0$, H = 3.7 km. To determine L and D information on elevation angle is needed. For purposes of illustration, the elevation angle is arbitrarily taken to be 42 deg. Then

$$L = \frac{H}{\sin\theta} = \frac{3.7}{0.669} = 5.53\ \text{km}$$

and

$$D = L\cos\theta = (5.53)\ (0.743) = 4.11\ \text{km}$$

4. The path reduction factor r_p for a probability of 0.01 is given by

$$r_p = \frac{1}{1 + 0.045\ D} \qquad \frac{1}{1 + 0.185} = 0.844$$

5. Total attenuation values A for p = 0.01 are calculated by using $A = \alpha_p L r_p$. For example

$$A_h = (0.660)\ (5.53)\ (0.844) = 3.08\ \text{dB}$$

where Ah is the attenuation for horizontal polarization. Values for vertical and, circular polarization, A_v and A_c respectively, are

$$A = 2.51\ \text{dB}$$

$$A_c^v = 2.79\ \text{dB}$$

The value for circular polarization is intermediate between values for horizontal and vertical polarization.

For circular polarization but for the rain rate exceeded for 0.1 percent of the time the attenuation $A_{0.1}$ is given by

$$A_{0.1} = A_{0.01}\ (0.12)\ p^{-(0.546\ +\ 0.043\ \log p)}$$

$$A_{0.1} = 2.79\ (0.12)\ 0.1^{-(0.546 + 0.043 \log 0.1)}$$
$$= 2.79\ (0.12)\ (3.184)$$
$$= 1.06\ \text{dB}$$

The value of attenuation exceeded for 0,1 percent of the time is smaller than that exceeded for 0.01 percent of the time.

9.4.3 Depolarization

9.4.3.1 Introduction

The degree of depolarization may be described in two principal ways. The terms cross polarization discrimination (XPD) and depolarization or cross polarization (D) have an inverse relation. The quantity XPD was defined by Eq. (4.32) as $20 \log (E_{11}/E_{12})$ where E_{11} is the copolarized or wanted signal and E_{12} is the cross polarized or unwanted signal which may have been produced by a process of depolarization. The term depolarization, however, may be used to represent 20 log (E_{12}/E_{11}). It can be noted that a high value of XPD, for example 40 dB, represents a favorable condition corresponding to a small value of D, namely -40 dB. Also the low value of XPD of 10 dB for example represents an unfavorable condition corresponding to the high value of D of - 10 dB.

For frequencies below about 10 GHz we favor the analysis by Chu (1980) for which depolarization D is given for circular polarization by

$$D_{cir}(\text{dB}) = 20 \log [\ 0.5\ [(\ \Delta\alpha_o)^2 + (\ \Delta\beta_o)^2]^{1/2}\ L \cos^2\theta\ e^{-2\sigma^2}]$$

(9.29)

For linear polarization, D is given by

$$D_{lin}(\text{dB}) = D_{cir}(\text{dB}) + 10 \log [0.5\ (1 - \cos 4\tau\ e^{-8\sigma^2_m})] \pm \Delta A'/2$$

(9.30)

In the above expressions $[(\Delta\alpha_o)^2 + (\Delta\beta_\theta)2]^{1/2}$ is the square root of the sum of the squares of the differential attenuation and phase constants (Fig. 9.11), L is the path length through rain, θ is the elevation angle of the path, and τ is the tilt angle from the horizontal of the electric field intensity of the linearly polarized wave. The quantity σ is the standard deviation of the raindrop canting angle ϕ, measured from the horizontal, along a path at a particular instant of time. As a conservative design procedure σ can be set equal to zero. The quantity σ_m is the standard deviation in radians of the mean raindrop canting angle ϕ_m from path to path and storm to storm. If ϕ_m is expressed in degrees, 8 σ_m^2 can be replaced by $\kappa_m^2 = 0.0024\ \sigma_m^2$ with 5 deg a suitable value for σ_m. The quantity AA' is given by

$$AA' = 5 \log (|\alpha_v|^2/|\alpha_h|^2)$$

where α_v and α_h are attenuation constants for vertically and horizontally polarized waves. The sign of $\pm\Delta A'$ should be chosen to give the lowest value of D for quasivertical polarization. In Eq. (9.30) the logarithm of a quantity less than unity is indicated and this logarithm is negative. Thus a linearly polarized wave has a smaller value of depolarization D than a circularly polarized wave. Equation (9.29) shows that depolarization decreases with increasing elevation angle. That polarization should decrease with increasing elevation angle can be understood by considering the outline of raindrops as seen from the direction of incident waves at $\theta = 0$ deg and at $\theta = 90$ deg. From the O deg direction the drops appear to have an elliptical shape, while from 90 deg the outline is circular. The elliptical cross section is conducive to depolarization, but the symmetrical circular cross section is not.

At frequencies above about 8 or 10 GHz, cross-polarization discrimination (XPD), the reciprocal of D, can be expressed in the form of U - V log A where A is attenuation in dB (CCIR, 1986e, 1986f). The basis for this form is developed in Sec. 4.4. We prefer to emphasize the application of Eqs. (9.29) and (9.30), however, as these are applicable over a large range of frequencies both above and below 10 GHz.

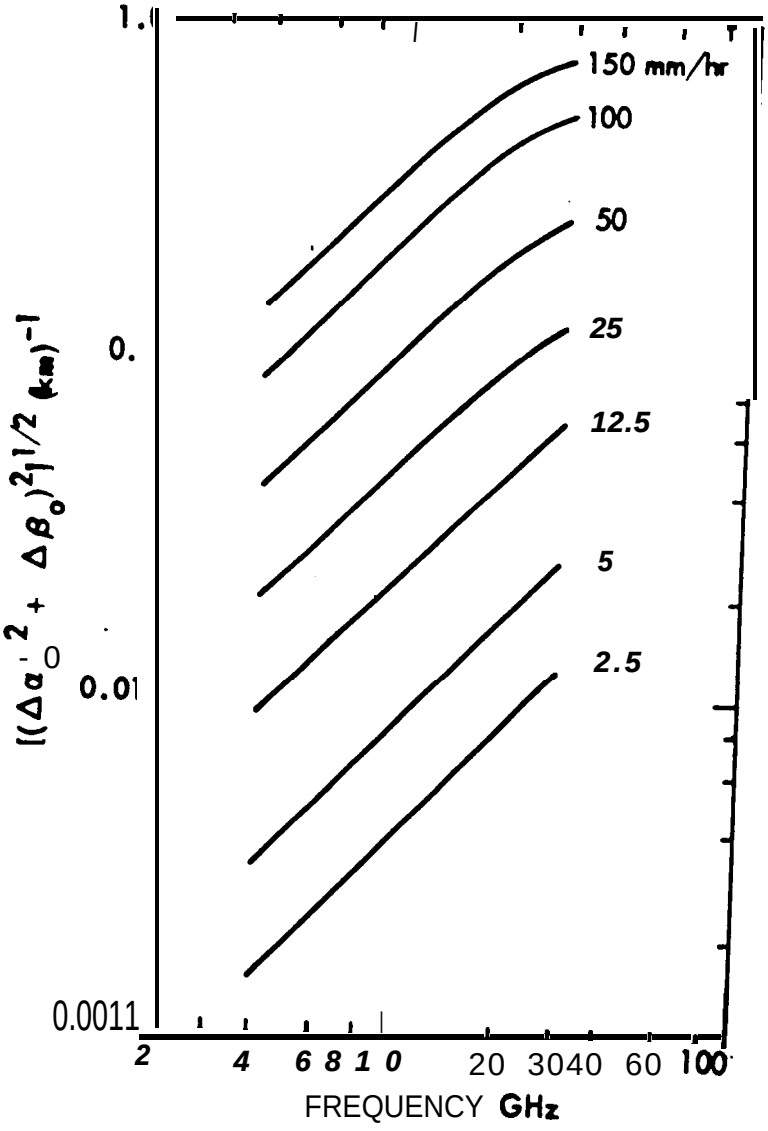

Figure 9.11. Calculated differential propagation constant at an elevation angle of zero degrees as a function of frequency for various rain rates (Chu, 1980).

Example 9.6 Depolarization at 8 GHz

This example compares depolarization for circularly and horizontal linearly polarized waves at a frequency of 8 GHz, an elevation angle of 42 deg, a latitude of 40 deg, and a rain rate of 50 mm/h. For this purpose, substitute the applicable values into Eqs. (9.29) and (9.30). From Fig. 9.11 for 8 GHz and 50 mm/h, a value of about 0.08 is found for the square root appearing in Eq. (9.29). In Example 9.5, for the same latitude and elevation angle, the path length L was found to be 5.53 km. Thus after substitution of values, Eq. (9.29) becomes

$$D_{cir}(dB) = 20 \log [(0.5) (0.08) (5.53) (0.552) 1$$
$$= 20 \log [0.122] = -18.27 \text{ dB}$$

Taking the tilt angle τ of Eq. (9.30) as O deg for horizontal polarization and using a value of 5 deg for σ_m results in

$$D_{lin}(dB) = -18.27 + 10 \log [0.5 (1 - \cos O'' e^{-0.0024 (25))}]$$
$$= -18.27 + 10 \log [0.5 (i - e^{- 0.06_{)1}} = -37.11 \text{ dB}$$

The quantity $\Delta A'/2$ was neglected above. If included the value of $D_{lin}(dB)$ turns out to be -36.61 dB. The depolarization is considerably smaller for the linearly polarized wave than for the circularly polarized wave. If the elevation angle of the path is reduced to 20 deg, the path length L becomes 10.3 km and $\cos^2\theta$ changes from 0.552 to 0.88 with the result that D_{cir} degrades from -18.27 dB to -8.37 dB.

9.4.3.3 Depolarization due to ice particles

Clouds above the O deg C isotherm consist at least in part of ice particles. These have a variety of shapes but are asymmetric and when they have a preferred orientation may cause depolarization not accompanied by appreciable attenuation (Bostian and Allnut, 1979; Cox, 1981). The depolarization in this case is produced primarily by differential phase shift. Rapid changes in depolarization due to ice prticles have been correlated with lightning strokes (Howell, 1977; McEwan et al., 1977). The relative amounts of rain and ice depolarization vary considerably with location and weather. When

attenuation is high, depolarization is due primarily to rain, but when depolarization is accompanied by only low values of attenuation a larger amount of the depolarization may be due to ice, except at the lower frequencies for which this handbook is aimed where depolarization may be primarily caused by differential phase shift even in the absence of ice. Chu (1980) has suggested the simple procedure of adding 2 dB to the depolarization caused by rain alone (subtracting 2 dJ3from XPD) in order to account for the effects of ice particles. Elsewhere it has been stated that an allowance of 2 dB may be sufficient for North America but that a value as much as . 4 or dB may be needed for the maritime climate of northwestern Europe (CCIR, 1986e).

9.4.3.4 Extrapolation of Data From One Path to Another

The analysis by Chu (1980) outlined in Sec. 9.4.3,2 and treated somewhat more fully in Sec. 4.4, allows extrapolation of depolarization D from one path to another having a different rain rate, frequency,. elevation angle, and polarization, For this purpose Chu uses

$$D_1(\mathrm{dB}) - D_2(\mathrm{dB}) = P_1 - P_2$$

$$+ 20 \log \left| \frac{[(\Delta\alpha_1)^2 + (\Delta\beta_1)^2]^{1/2} \cos^2\theta_1 \, L_1}{[(\Delta\alpha_2)^2 + (\Delta\beta_2)^2]^{1/2} \cos^2\theta_2 \, L_2} \right| \qquad (9.31)$$

where the P's represent polarization factors which are zero for circular polarization and for linear polarization are given by

$$P = 10 \log [\, 0.5 \, (1 - \cos 4\tau e^{-8\sigma_m})] \pm \Delta A'/2 \qquad (9.32)$$

The quantities L_1 and L_2 are the two path lengths through rain. The factors appearing in Eqs. (9.3 1) and (9.32) have the same meanings as in Eqs. (9,29) and (9.30) and take account of the same difference between linear and circular polarization.

Figure 9.12 shows the application of the procedure outlined to comparison of depolarization at 4 GHz for linearly polarized transmissions on a path with an elevation angle of 38.6 deg in New

Jersey with depolarization on a path with an elevation angle of 9 deg in Japan where circular depolarization was employed.

Further information on the low values of XPD (high values of D) which may be encountered at the low elevation angles utilized on some 4 GHz earth-space paths from Japan is shown in Fig. 9.13 (Kobayashi, 1976). Low values of XPD have also been reported by Taur (1974) at 4 GHz on paths terminating at Washington, DC and having 'higher elevation angles.

Example 9.7 Comparison of Depolarization for Different Paths

The application of Eq. (9.32) to the comparison of depolarization on two different paths will now be illustrated. Let Station 1 have an elevation angle of 10 deg and circular polarization. Let Station 2 have an elevation angle of 40 deg and quasivertical polarization with a tilt angle τ of 75 deg. Assume that both stations operate at 4 GHz, that Station 2 is reported to have a depolarization of -30 dB, and that it is desired to determine the depolarization of Station 1. The comparison will be made for the same rain rate of 35 mm/h at both stations. Station 1 can be expected to have a higher depolarization (less favorable for frequency sharing) than Station 2 so that $D_1 - D_2$ should be positive.

As Station 1 has circular polarization, P_1 is zero. [See Eqs. (9.29) and (9.30).] The principal term of P_2 is

$$10 \log[0.5(1 - \cos 4\tau\, e^{-8\sigma_m^2})] = 10 \log[0.5(1 - \cos 300^\circ\ 0.942)]$$

$$= -5.77 \text{ dB}$$

where the exponential term has the same value as in Example 9.6. By using values of a_H, a_V, b_H, and b_v from Table 9.9 it is determined that AA/2 is 1.19. Therefore

$$P_1 - P_2 = 0 - (-5.77 - 1.19) = 6.96$$

Considering next the second term of Eq. (9.31), the propagation constants are the same if the same rain rate is assumed and the difference in depolarization due to this term is

$$20 \log \left[\frac{\cos^2\theta_1 L_1}{\cos^2\theta_2 L_2} \right] = 20 \log \left[\frac{\cos^2 10^\circ\ (1/\sin 10^\circ)}{\cos^2 40^\circ\ (1/\sin 40^\circ)} \right]$$

$$= 15.73$$

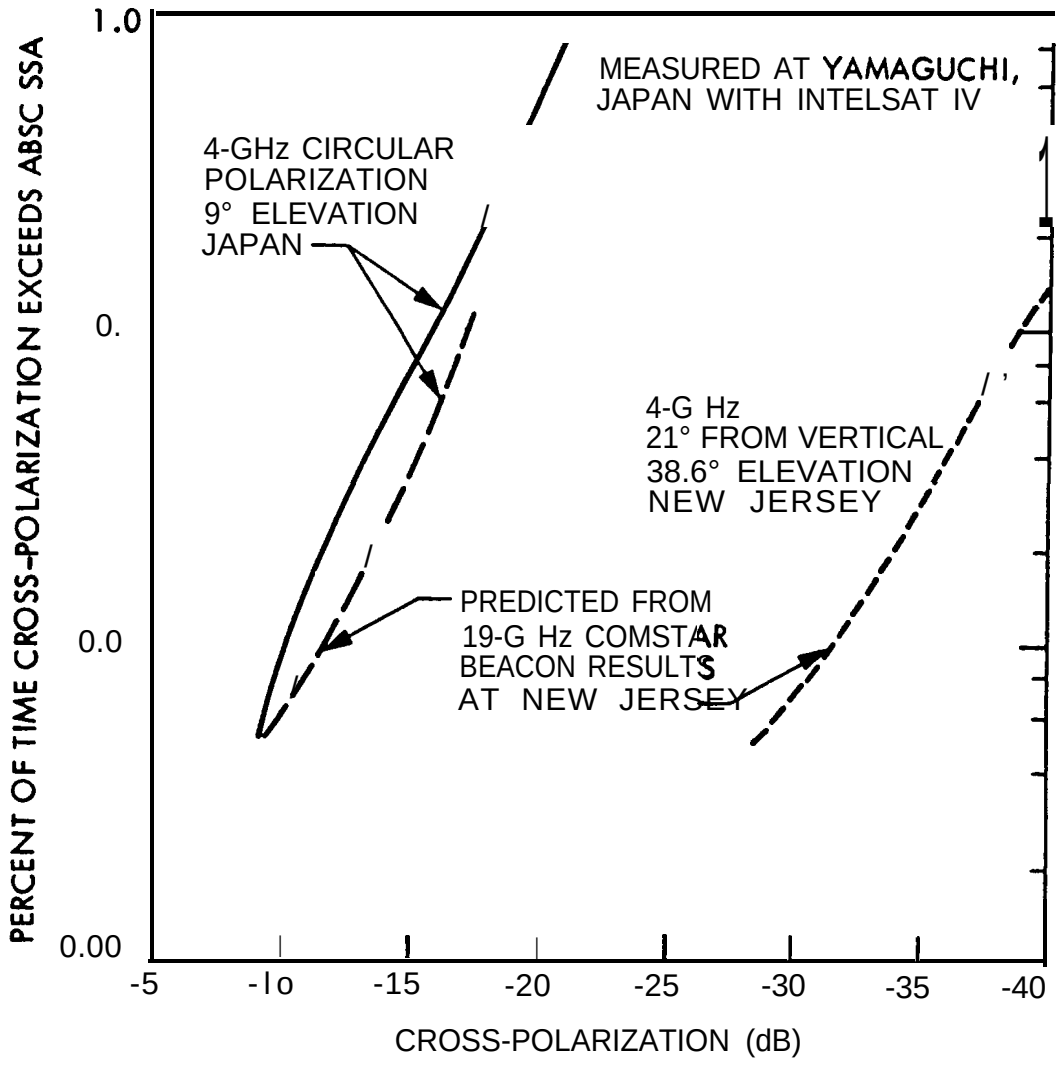

Figure 9.12. Comparison between measured 4 GHz circularly polarized INTELSAT IV depolarization statistics at 9 deg elevation angle and prediction from COMSTAR measurements (Chu, 1980).

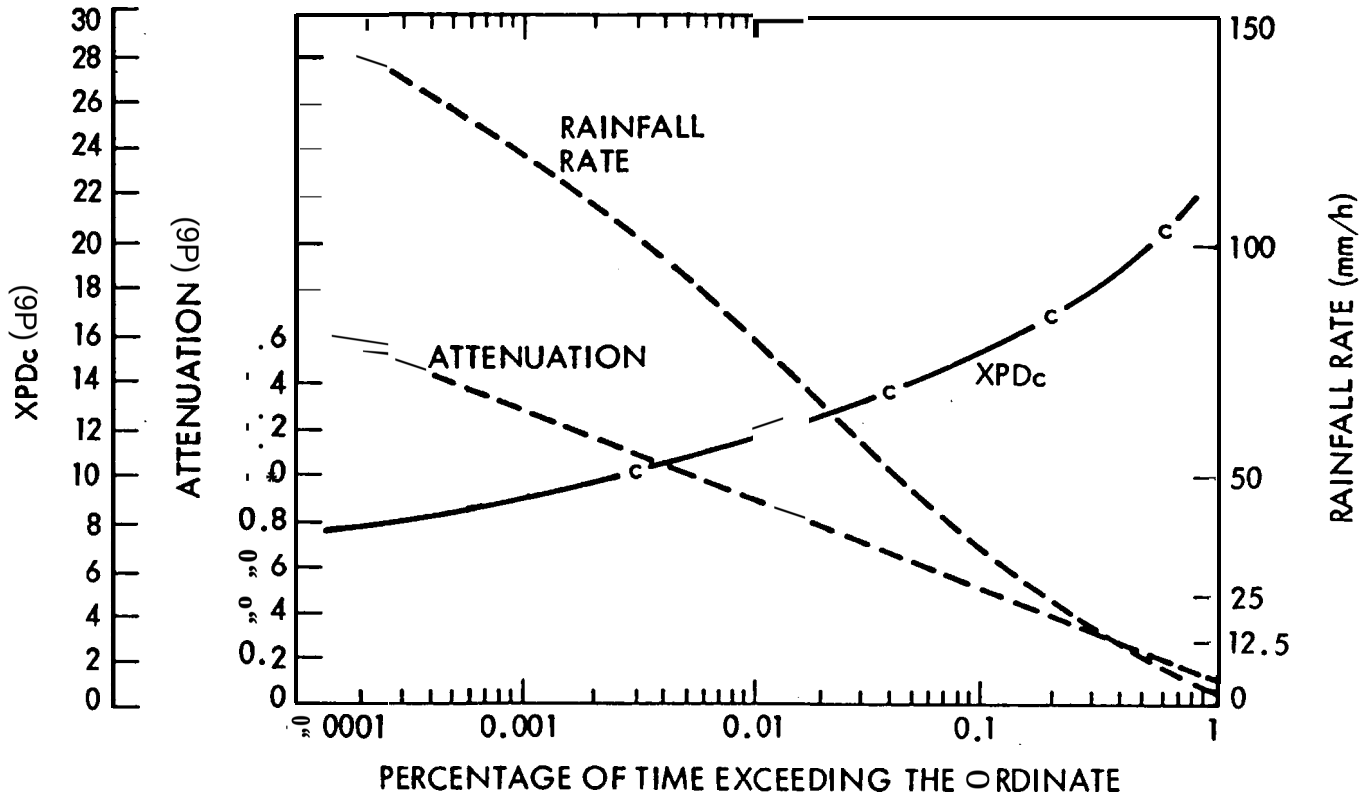

Figure 9.13. Pre-estimation of XPD on a satellite communication circuit, 4 GHz, 8 deg elevation angle, circular polarization, Yamaguchi station (Kobayashi, 1976).

Thus

$$(D_1)_{dB} - (D_2)_{dB} = 6,96 + 15.73 = 22.69 \text{ dB}$$

and

$$(D_1)_{dB} - (-30) = 22.69$$

$$(D_1)_{dB} = 22.69\text{-}30 = -7.31 \text{ dB}$$

To take account of different frequencies or rain rites use can be made of Fig. 9.11. For example if Station 2 operated at 8 GHz with the same depolarization of -30 dB, but Station 1 remained at 4 GHz, the ratio of propagation constants of Eq. (9.31) would be roughly 1/2 and in place of 1 5.73 for the second term of Eq. (9.31) one would have about 9.7. Then $(D_1)_{dB}$ would be about -13.3.

Note that whereas Station 2 was known to operate with a depolarization of -30 dB (XPD of +30 dB), Station 1, at the same frequency and rain rate in the original case considered but having a different path, was predicted to have the clearly unsatisfactory D value of -7.3 dB (XPD of +7.3 dB).

9.5 EFFECTS OF CLOUDS, DUST, AND VEGETATION

Attenuation due to clouds is normaly no greater than 0.5 dB for a vertical path for frequencies of 10 GHz and less. For the same conditions otherwise, the attenuation would be 1 dB for an elevation angle of 30 deg and 2.88 dB for an elevation angle of i O deg if the attenuation were 0.5 dB for a vertical path. As every dB of attenuation may be important, clouds may be of significance for frequencies as low as 10 GHz and somewhat lower, as well as for higher frequencies for which the attenuation is greater. Also as was indicated for the case of rain, dissipative attenuation is accompaied by an increase in noise and both effects contribute to a degradation in signal-to-noise ratio. Section 9,7 and Chap. 7 specify and discuss further the relation between attenuation and noise. Table 7.1 gives attenuation and noise temperature values for 12 different cloud 'models.

Although effects due to clouds do not become as intense as those due to rain, they occur for larger percentages of time. For operations for which propagation impairments occurring for

relatively high percentages of the time, such as 1 to 10 percent or greater, are pertinent (rather than or in addition to small percentages such as 0.01), the effects of clouds assume the greatest relative importance. In a study of effects of clouds by Slobin (i 982), the United States has been divided into 1 5 regions shown in Fig. 9.14. For these regions data on cumulative distributions of zenith atmospheric noise temperatures due to clouds have been provided. Figure 9.15 shows such distributions for 5 of the 15 regions.

Only very limited data on attenuation due to sand and dust are available. For earth stations in desert areas where serious sand or dust storms occur, an allowance of 1 dB for attenuation due to sand and dust on an earth-space path may be advisable.

Section 5.3 includes some background material on the effects of vegetation on propagation, primarily from one point on the Earth's surface to another. An empirical expression developed by Weissberger for attenuation due to small groves of trees has the form, as simplified in CCIR Report 236-6, of

$$A_{dB} = 0.20\, f^{0.3} d^{0.6} \qquad (9.33)$$

with frequency f in MHz and distance d in meters. Recent data on attenuation on simulated earth-space paths are given in Chap. 6 and commented on briefly in the following Sec. 9.6.

9.6 PROPAGATION EFFECTS ON MOBILE SYSTEMS

Propagation effects on earth-space paths utilized for communication with land vehicles, ships, and aircraft include specular reflection, diffuse scatter, and shadowing by vegetation. Example 9.8 deals with reflection coefficients for reflection of linear and circularly polarized waves. Studies carried out by simulating conditions on earth-space paths have shown the importance of shadowing by trees, including even single trees. Attenuation values are generally higher for these paths than the values given by the empirical expression of Sec. 9.5 which was developed for ground-to-ground paths. A sizeable margin of over 10 dB may be advisable for attenuation due to roadside trees (Sec. 6.4). Interstate highways have wider cleared areas and tend to be less afffected than two-lane roads or parkways. Attenuation is encountered, however, when driving through underpasses. Recently

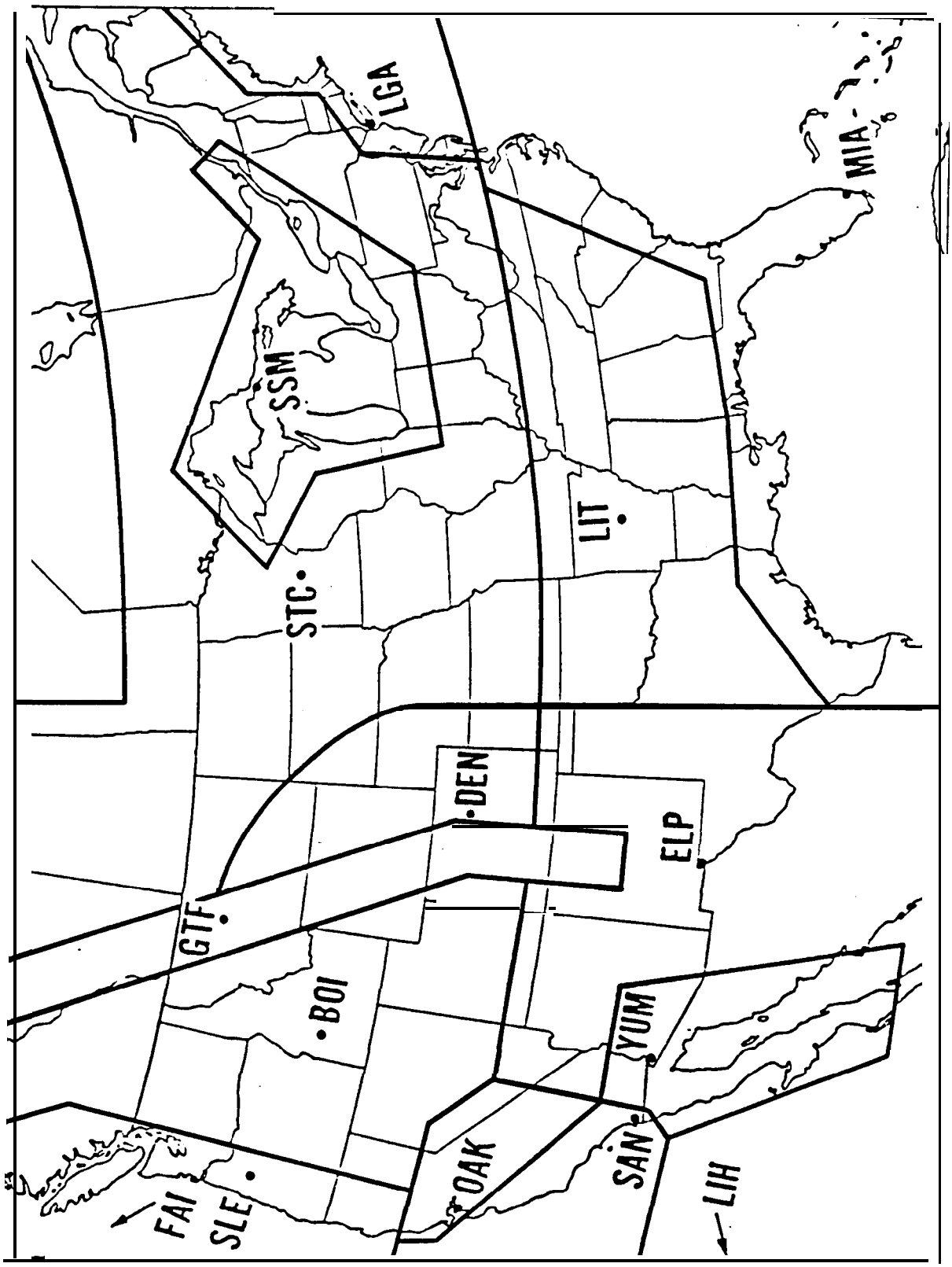

Figure 9.14. Cloud regions of the United States (Slobin, 1982).

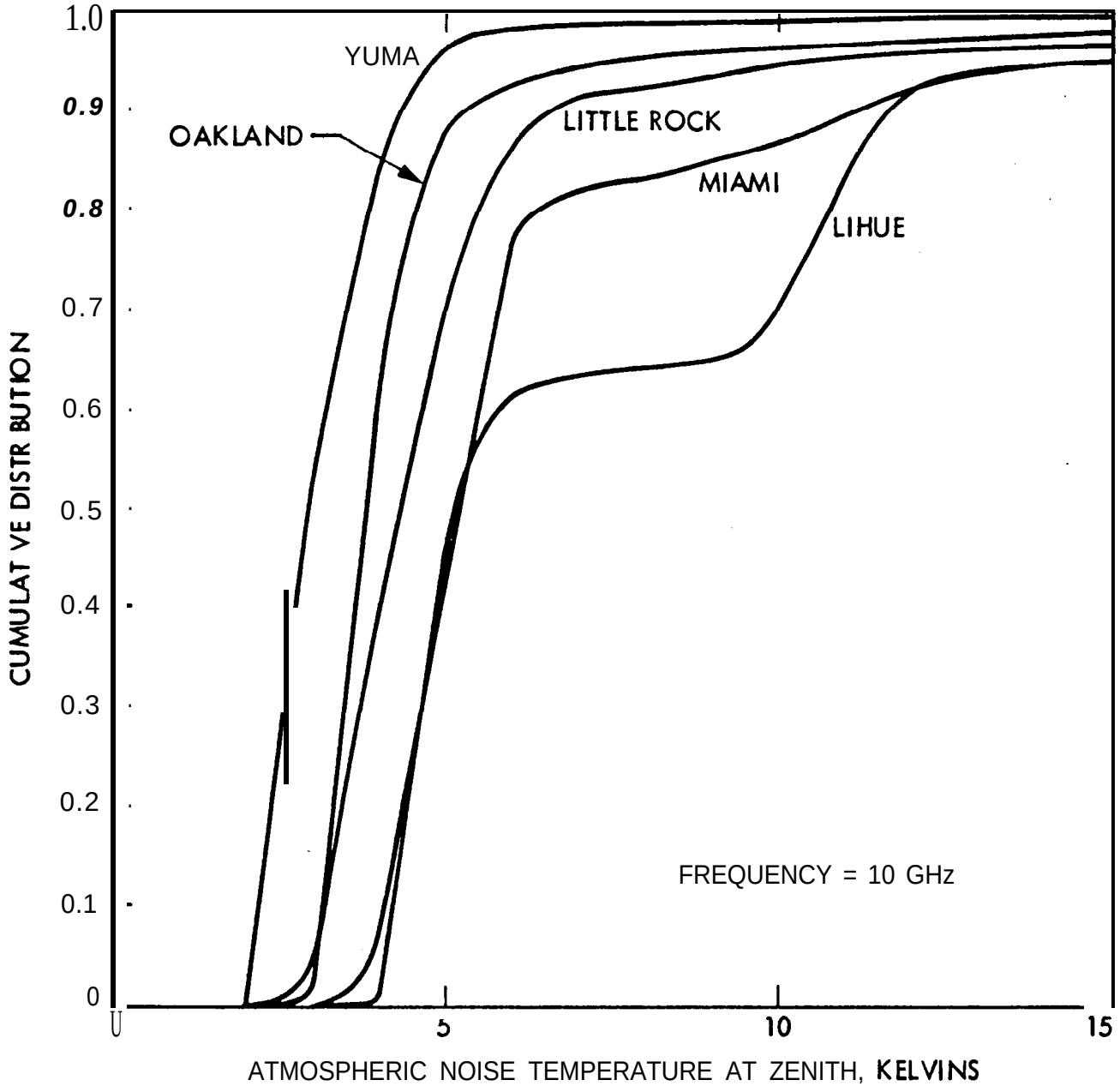

Figure 9.15. Total-year cumulative distributions of zenith atmospheric noise temperature for five regions at 10 GHz (Slobin, 1982).

reported studies by Vogel, Torrence, Goldhirsh, and Rowland (1987) in Colorado show only very small effects from reflections from canyon walls. Interesting periodic signal fades were recorded due to reflection from roadside power-line poles in open country.

Example 9.8 Reception of Signals from Geostationary Satellites by Land-Mobile Receivers.

The transmission of circularly polarized waves at a frequency of 1000 MHz is featured in this example. Calculations are made for two elevation angles, 10 deg and 30 deg. Possible ionospheric effects are neglected, but ionospheric scintillation would need to be taken into account at low latitudes. Average ground (relative dielectric constant K = 15 and conductivity y σ = 0,005 mhos/m) is assumed. Calculations are included for h_s = 0.1 m, where h_s is the rms height of irregularities, and for a perfectly smooth surface for which h_s = O.

Notation:

ρ_h, ρ_v are smooth-earth reflection coefficients for horizontal and vertical polarization. They are calculated by using Eqs. (6. 14), (6. 15).

ρ_c, ρ_x are smooth-earth reflection coefficients for the copolarized and crosspolarized components of the reflected wave and are given by Eqs. (6. 18) and (6. 19).

ρ_s is a surface roughness factor given by Eq. (6.28).

ρ_{cs}, ρ_{xs} are rough-surface reflection coefficients defined by

$$\rho_{cs} = \rho_c \rho_s \text{ and } \rho_{xs} = \rho_x \rho_s$$

ρ_d isa diffuse reflection coefficient.

θ is elevation angle,

g_{cr} is the relative (normalized) voltage gain of the receiving antenna for the co-polarized component of the reflected wave.

g_{xr} is the relative voltage gain for the cross-polarized component of the reflected wave.

The surface roughness factor ρ_s is given by

$$\rho_s = e^{-(\Delta\phi)^2/2}\, I_0[(\Delta\phi)^2/2]$$

with

$$\Delta\phi = 4\pi (h_s/\lambda) \sin\theta$$

Specular Reflection: Elevation Angle $\theta = 10^\circ$

Use of Eqs. (6. 14) and (6.15) gives a value for ρ_h of -0.91 and a value for ρ_v of -0.18. Then

$$P_c = (\rho_h + \rho_v)/2 = (-0.91-0.18)/2 = -0.55$$

$$\rho_x = (\rho_h - \rho_v)/2 = (-0.91 + 0.18)/2 = -0.37$$

$$\rho_s = 0.783 \text{ for } h_s = 0.1 \text{ m}$$

$$P_{cs} = (0.783)(-0.55) = -0.431$$

$$P_{xs} = (0.783)(-0.37) = -0.290$$

The incident wave has only pure right or left circular polarization, but the reflected wave has a combination of both types with the original polarization dominant. Interest here is in the combination of the direct wave and the comporients of the specularly reflected wave. Account must be taken of the normalized voltage gains g_{cr} and g_{xr} -of the receiving antenna as a function of angle from that of the direct ray. The angle of the reflected rays differs from that of the direct ray by 2θ where θ is elevation angle. If the gains of the receiving antenna are known as a function of angle, they should be used. Here it is arbitrarily assumed that the gain g_{cr} for the copolarized reflected wave, differing by 20 deg from that of the direct wave, is 3 dB down from that for the direct wave, while the gain g_{xr} is 9 dB down. Then the relative magnitude of the total signal can be expected to fall within the limits of

$$1 \pm [|g_{cr}(20^\circ)|\,|\rho_{cs}| + |g_{cr}(20^\circ)|\,|\rho_{xs}|] = 1 \pm 0.407$$

which corresp ends to a variation, relative to the signal for the direct wave alone, of +2.96 to -4.53 dB.

The value for a perfectly smooth earth is obtained by using ρ_c and ρ_x instead of ρ_{cs} and ρ_{xs}. The limits of the normalized field intensity in this case are 1 ± 0.519 or +3.63 to -6.35 dB.

Specular Reflection; Elevation Angle $\theta = 30°$

The reflection coefficients for horizontal and vertical polarization in this case are -0.77 and +0.33, respectively. The Brewster angle [angle of minimum reflection coefficient as given by Eq. (6.15)] is $\tan^{-1} 1/(K_2)^{1/2} = \tan^{-1} 1/(15)^{1/2} = 14.48$ deg in this case. The elevation angles of 10 and 30 deg are on opposite sides of the Brewster angle and the sign of the reflection coefficient for vertical polarization is different on the two sides. The result is that ρ_x now becomes larger than ρ_c as indicated by

$$P_c = (\rho_h + \rho_v)/2 = -0.22$$

$$\rho_x = (\rho_h - \rho_v)/2 = -0.55$$

The roughness factor ρ_s for 30 deg is smaller than for 10 deg. In particular

$$\rho_s = 0.290$$

so that

$$\rho_{cs} = (0.290)\ (-0.22) = -0.064$$

$$\rho_{xs} = (0.290)\ (-0.55) = -0.160$$

Although antennas are designed to have much larger gain for the copolarized wave than for the crosspolarized wave for the center of the main beam (boresight), their gains at a large angle from the center may be about the same. For the present case, it is assumed that both g_{cr} and g_{xr} are 10 dB down from the gain at the center of the beam. For this condition and still for $h_s = 0.1$ m, the total normalized signal should fall within the limits of

$$1 \pm g_r(0°)\ [|\rho_{cs}| + |\rho_{xs}|] = 1 \pm 0.070 \text{ or } +0.59 \text{ to } -0.63 \text{ dB}$$

For a perfectly smooth earth, the corresponding values are +1.89 to -2.42 dB.

The fading is only about 2.4 dB for a smooth earth. Now assume that g_r(60 deg) = 1. That is, assume that the normalized gain at an angle of 60 deg from boresight is the same as on boresight. The result for a smooth earth is that the total signal variation falls in the range of 1 ± 0.77 or +4.95 to -12.8 dB. The values are not realistic but are mentioned to show the importance of antenna discrimination in minimizing the role of multipath effects in mobile communication. With discrimination of 10 dB for both the copolarized and crosspolarized wave components, fading is reduced from 12.8 dB to 2.4 dB for the case of a smooth earth.

Returning to the case of surface roughness, specular reflection decreases and diffuse scatter increases as roughness increases. The combination of specular reflection and diffuse scatter tends to be described by the Rician distribution, shown in Fig, 6.11 as function of diffuse reflection coefficient ρ_d. Fading due to shadowing by vegetation or otherwise, however, follows the log-normal distribution. Fading on simulated earth-space paths tends to show a combination of Rician and log-normal fading (Fig. 6, 16). The phenomena of specular reflection and diffuse scatter need to be understood and taken into account, but shadowing by vegetation has come to assume a dominant role in consideration of what margins are needed in land-mobile satellite service.

9.7 RADIO NOISE

9.7.1 Basic Relations

The system noise temperature, T_{Sys}, and the noise temperature, T_s, of Fig. 9.16 are given by

$$T_{Sys} = T_A + (l_a - 1)T_o + l_a T_R \qquad (9.34)$$

and

$$T_s = T_A g_a + (1 - g_a)T_o + T_R \qquad (9.35)$$

In these equations, T_A is the antenna noise temperature, T_0 is the

attenuator temperature, normally taken as 290 K, and T_R is the receiver noise temperature. The factor g_a is the attenuator "gain" and has a maximum value of one; the factor l_a equals $1/g_a$ and has a minimum value of one. If there is no attenuation, $T_{Sys} = T_s = T_A + T_R$

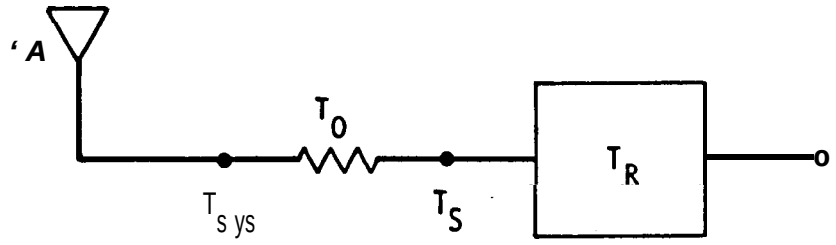

Figure 9.16. Noise temperatures of a receiving system.

The brightness temperature T_b, recorded when observing a noise source T_s through an absorbing region having an intrinsic temperature T_i and causing an attenuation represented by $e^{-\tau}$ is given by

$$T_b = T_s e^{-\tau} + T_i(1 - e^{-\tau}) \qquad (9.36)$$

Note that g_a and $e^{-\tau}$ are alternative ways of representing attenuation and that if $T_R = 0$, Eqs. (9.35) and (9.36) are identical in form. Attenuation in an attenuator is represented here by g_a and that in the atmosphere is represented by $e^{-\tau}$. In both cases attenuation is encountered and thermal noise is generated in an absorbing medium.

In the case of an earth station receiving system, T_A may be approximately equal to T_b. That is, the antenna noise may be primarily that due to an absorbing region along the path plus perhaps noise of distant origin that is attenuated by the absorbing region. Actually other noise sources, such as terrestrial noise picked up by the antenna sidelobes and backlobe make at least a small contribution to to T_A as well, In some situations the value of the term Ts may be negligible and

$$T_b = T_i(1 - e^{-\tau}) \qquad (9.37)$$

Also absorption may be negligible in some cases and then $T_b = T_A = T_S$" Consider that a signal is propagating through an absorbing region, for example a region where rain is falling. The signal is attenuated by a factor of' $e^{-\tau}$ or by A_{dB} where $A_{dB} = 4.34\ \tau$. Also the antenna receives noise given by Eq. (9.37). Values of T_i have been determined and found to range mostly from 260 to 290 K. The degradation in signal-to-noise ratio, C/X, compared to the case when no absorption occurs along the path is given by

$$\Delta(C/X)_{dB} = A_{dB} + 10 \log (T_2/T_1) = A_{dB} + 10 \log [(T_1 + T_b)/T_1] \qquad (9,38)$$

where T_1 is the system noise temperature in the absence of the absorbing region and $T_2 = T_1 + T_b$ is the temperature in the presence of the absorbing region.

The concept presented here applies regardless of what the absorptive attenuation is due to (rain, clouds, or atmospheric gases). Note that the magnitude of 10 log (T_2/T_1) with $T_2 = T_1 + T_b$ depends on the relative magnitudes of T_1 and T_b. If T_1 is large, a given value of T_b tends to cause a relatively small change in T_2/T_1, but if T_1 is small the same value of T_b causes a larger change in T_2/T_1. For low-noise systems and for attenuations up to about 10 dB, the degradation in the C/X ratio due to noise may be larger than that due to attenuation (Fig. 9. 17).

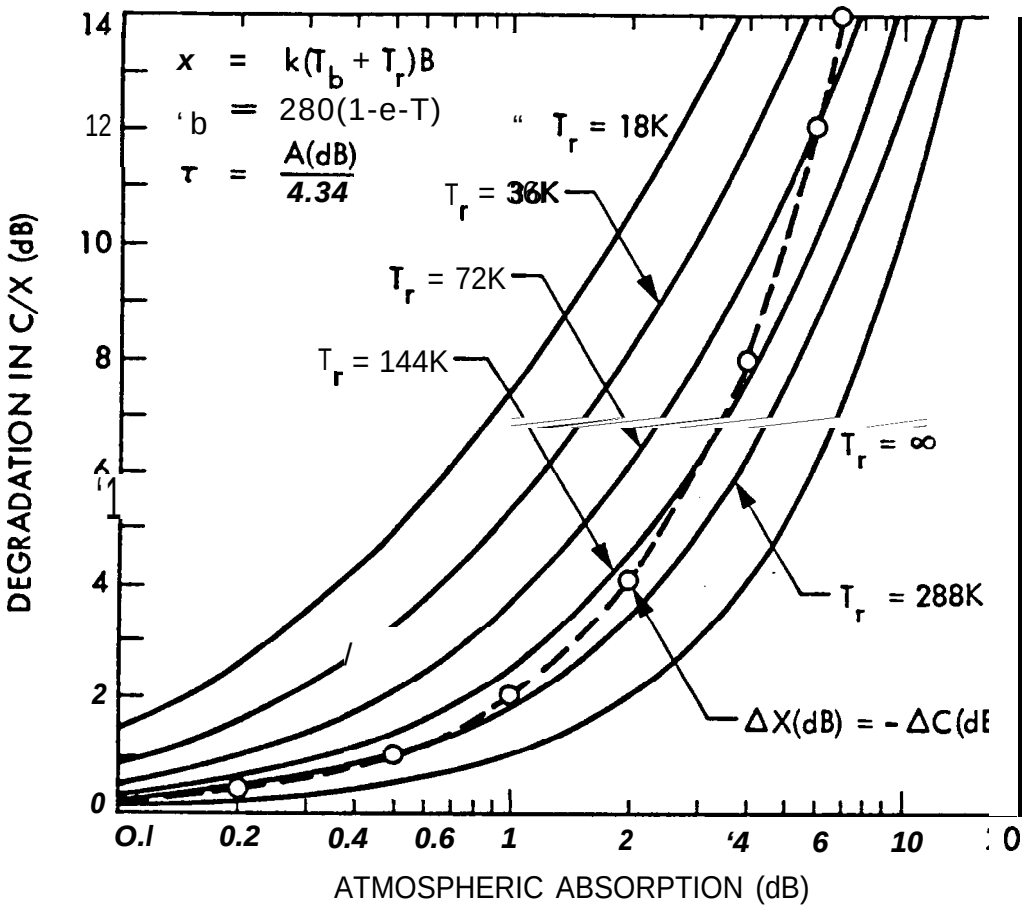

Figure 9.17. Degradation in signal-to-noise ratio (C/X) versus atmospheric absorption, for various values of T_1 (with T equal to T_r).

9.7,2. Noise Sources

9.7.2.1 Extraterrestrial Noise

In the lower decade of the frequency range of this handbook from 100 MHz to 1000 MHz (1 GHz), extraterrestrial (cosmic) noise is the dominant type of noise. Atmospheric thermal noise dominates above 10 GHz, and the frequency range from 1 to 1 O GHz has the least noise of natural origin of the radio-frequency spectrum,

The most intense extraterrestrial radio noise sources other than the Sun are non-thermal and have positive spectral indices, which means that their noise powers increase with wavelength and decrease with frequency. Figure 7.11 shows radio emission from that part of the celestial sphere of interest to satellite operations employing the geostationary orbit (declination angles from +8.7 to -8.7 deg) and includes data for larger declination angles as well. The plot is in celestial coordinates with declination angle δ measured from the celestial equator which is an extension into space of the Earth's equator. Declination angles of $\pm$ 8.7 deg correspond to the highest possible latitudes ($\pm$ 81.3 deg) which can be used for communication with geostationary satellites. For an earth station in the northern hemisphere at a latitude of 9', the extraterrestrial noise received is that from a strip of sky behind the satellite having a declination angle δ given by

$$\delta = -\tan^{-1}\left(\frac{\sin\theta'}{6.6 - \cos\theta'}\right) \qquad (9.39)$$

and equals -6,3 deg for $\theta' = 40$ deg. The fraction within the brackets of Eq. (9.39) is a ratio of distances measured in earth radii, geostationary satellites being at 6.6 earth radii from the center of the Earth. By examination of Fig. 7.11 (or a better original version) and from the accompanying discussion of Chap. 7, it can be determined that the maximum noise temperature at 250 MHz for an earth station at a latitude of 40 deg that is communicating with a geostationary satellite is 850 K. For other frequencies an equivalent blackbody temperature T can be determined by assuming that T varies as f^{-2+n} where n is the spectral index and can be taken as 0.75 as in Sec. *7.3.4* (Smith, 1982a). In adddition, for microwave frequencies, the microwave

background temperature of 2.7 K should be included in T_b, the total brightness temperature. Thus for a microwave frequency f_i

$$T_b(f_i) = T_b(f_o)(f_i/f_o)^{-2.75} + 2.7 \text{ K} \qquad (9.40)$$

with f. equal to 250 MHz.

9.7.2.2 Atmospheric Thermal Noise

Thermal noise generated by the atmospheric gases, clouds, and rain is related to attenuation in these same media by Eqs. (9.36) and (9.37) of Sec. 9,7.1. Knowledge of attenuations and the intrinsic temperatures of the media allow estimation of noise temperatures.

Detailed analyses of the attenuation and noise due to gases (Smith, 1981, 1982b) and clouds (Slobin , 1981, 1982) have been prepared. Values of attenuation due to gases are shown in Fig. 3.11 and discussed in Sec. 9.3. Table 5.3 provides some data on attenuation and atmospheric thermal noise due to clouds, and Table 7.1 presents more detailed information on the same topics. For many purposes the attenuation and noise due to the gases can be neglected for frequencies of 10 GHz and lower, but for low-angle paths and for coordination-area analyses the effects of oxygen may need to be taken into account. As discussed in Sec. 9.5, the effects of clouds may be of some significance for frequencies of 10 GHz and somewhat lower.

9.7.2.3 Terrestrial Noise

In the past it has commonly been assumed that, for the uplink to a satellite, the receiving antenna points at the ground and therefore should be assigned a noise temperature of 290 K. However, analysis of the problem by Njoku and Smith (1985) has shown that the noise temperature may be considerably lower, especially at frequencies of 10 GHz and lower, as shown in Fig. 7.14. The receiving antenna of a downlink from a satellite points at the sky but nevertheless picks up at least a small amount of terrestrial noise, ranging from one or a few degrees for a very-high-quality antenna to tens of degrees or more.

Example 9.8 Decrease in Signal-to-Noise Ratio Caused by Absorbing Region

a. Consider a receiving system with a system noise temperature $T_{Sys} = T_1 = 100$ K in the absence of attenuation along the transmission path. Assume then that an attenuation of 1 dB occurs along the path in an absorbing region where the intrinsic temperature is 280 K. Because of the absorbing region T_{sys} increases to a new value T_2. The temperature T_2 and the total decrease in signal-to-noise-ratio winnow be calculated. The relation between T of $T_b = T_i(1 - e\text{-}r)$ and attenuation A is

$$\tau = A_{dB}/4.34$$

For this case, $\tau = 1/4.34 = 0.23$ and $e^{-\tau} = 0.794$. Thus

$$T_b = 280\ (1 - 0.794) = 57.6\ \text{K}$$

and from Eq. (9.38)

$$\Delta(C/X)_{dB} = 1 + 10 \log \frac{100 + 57.6}{100}$$

$$= 1 + 1.98 = 2.98\ \text{dB}$$

b. Next let $T_1 = 25$ K, with other conditions the same as in part a.

$$\Delta(C/X)_{dB} = 1 + \text{lo} \log \frac{25 + 57.6}{25}$$

$$= 1 + 5.19 = 6.19\ \text{dB}.$$

The total decrease in C/X is over six times that due to attenuation.

c. For the attenuation due to rain of 2.79 dB, found for circular polarization in Example 9.5, with $T_1 = 100$ K,

$$\tau = 2.79/4.34 = 0.643 \text{ and } e^{-\tau} = 0.525$$

$$T_b = 280(1 - 0.525) = 132.78\ \text{K}$$

$$\Delta(C/X)_{dB} = 2.49 + 10 \log \frac{100 + 132.78}{100}$$

$$= 2.79 + 3.67 = 6.45\ \text{dB}$$

REFERENCES

Aarons, J., I-I.E. Whitney, E. Mackenzie, and S. Basu, "Microwave equatorial scintillation intensity during solar maximum, " Radio Sci., vol. 10, pp. 939-945, Sept.-Oct. 1981.

Aarons, J., "Global morphology of ionospheric scintillations," Proc. IEEE, vol. 70 pp. 360-378, April 1982.

Bean, B.R. and E.J. Dutton, Radio Meteorology. Washington, DC: Supt. of Documents, U.S. Gov't Printing Office, 1966,

Bostian, C.W. and J.E. Allnut, "Ice-crystal depolarization on satellite-earth microwave radio paths," Proc. IEEE, vol. 126, p. 951, 1979.

CCIR, Report 263-5, 1982. [Earlier version of CCIR (1986 a)]-

CCIR, "Ionospheric effects upon earth-space propagation," Report 263-6, Vol. VI, Propagation in Ionized Media, Recommendations and Reports of the CCIR, 1986. Geneva: Int. Telecomm. Union, 1986a.

CCIR, "Effects of lame-scale tropospheric refraction on radiowave propagation," Report 718-2, Vol. V, Propagation in Non-ionized Media, Recommendations and Reports of the CCIR 1986 Geneva: Int. Telecomm. Union. 1986b.

CCIR, "Radiometeorological data," Report 563-3, Vol. V, Propagation in Non-ionized Media, Recommendations and Reports of the CCIR, 1986. Geneva: Int. Telecomm. Union, 1986c.

CCIR, "Attenuation by hydrometers, in particular precipitation, and other atmospheric particles, " Report 721-2, Vol. V, Propagation in Non-ionized Media Recommendations and Reports of the CCIR, 1986. Geneva: Int. Telecomm. Union, 1986d.

CCIR, "Propagation data required for space telecommunication systems," Report 564-3, Vol. V, Propagation in Non-ionized Media Recommendations and Reports of the CCIR, 1986. Geneva: Int. Telecomm. Union. 1986e.

CCIR, "Cross-polarization due to the atmosphere," Report 722-2, Vol. V, Propagation in Non-ionized Media, Recommendations and Reports of the CCIR, 1986. Geneva: Int. Telecomm. Union, 1986f.

Chu, T. S., "Microwave depolarization of an earth-space path," Bell System Tech. Jour., vol. 59, pp. 987-1007, July-Aug. 1980.

Cox, D. C., "Depolarization of radio waves by atmospheric hydrometers in earth-space paths: a review," Radio Sci., vol. 16, pp. 781-812, Sept.-Ott, 1981.

Crane. RK.. "Refraction effects in the neutral atmosphere," in Methods "of Experimental Physics, vol. 12, Astrophysics, Part B: Radio Telescopes (M.L. Meeks, ed.), pp. 186-200. New York: Academic Press, 1976.

Crane, R. K., "Prediction of attenuation by rain," IEEE Trans. Commun., vol. COM-28, pp. 1717-1733, Sept. 1980a.

Crone, R. K., "Earth-space and terrestrial microwave propagation - estimation of rain attenuation with the global model," ERT Tech. Report P-A4 14-TR prepared for NASA, Oct. 1980b.

Davies, K., Ionospheric Radio Propagation. Washington, DC: Sup. of Documents, U.S. Gov't Printing Office, 1965.

Davies, K., "Recent progress in satellite radio beacon studies with particular emphasis on the ATS-6 radio beacon experiment ," Space Sci. Rev., vol. 25, pp. 357-430, April 1980.

Dawson, E. and L.R. Newitt, "The magnetic poles of the Earth," J. Geomag. Geoelectr., vol. 34, no. 4, pp. 225-240, 1982.

Fang, D. J., F.T. Tseng, and T.O. Calvit, "A low elevation angle propagation measurement of 1.5-GHz satellite signals in the Gulf of Mexico," IEEE Trans. Antennas Propagat., vol. AP-30, pp. 10-15, Jan. 1982.

Flock, W. L., "Propagation at 36,000 Mc in the Los Angeles basin," IRE Trans. Antennas Propagat., vol AP-8, pp. 235-241, May 1960.

Flock, W.L., S.D. Slobin, and E.K. Smith. "Propagation effects on radio range and noise in earth-space telecommunications," Radio Sci., vol. 17, pp 1411-1424, Nov.-Dee. 1982.

Fremouw, E. J., "A computer model of high-latitude scintillation," 82-0150, Tech. Papers, Aerospace Sci. Meeting, Orlando, FL, Jan. 11-14, 1982, 9 pp. New York: AIAA, 1982.

Fremouw, E.J. et al., "The HiLat satellite mission," Radio Sci., vol. 20, pp.416 -424, May-June 1985.

Hopfield, HS ., "Tropospheric effect On electromagnetically measured range: predict ion from surface weather data," Radio Sci., vol. 6, pp. 357-367, March 1971.

Howell, R, G., "Cross-polar phase variations at 20 and 30 GHz on a satellite-earth path," Electr. Lett., vol. 1 3> pp. 405-406, 1977.

Ippolito, L. J., R.D. Kaul, and R.G. Wallace, Propagation Effects Handbook for Satellite Systems Design, A Summary of Propagation Impairments on 10 to 100 GHz Satellite Links With Techiques for System Design, NASA Reference Pub. 1082(03), Washington, DC: NASA Headquarter, i 983.

Karasawa, Y., K. Yasukawa, and M, Yamada, "Ionospheric scintillation measurements at 1. 5 GHz in mid-latitude region," Radio Sci., vol. 20, pp. 543-551, May-June 1985.

Klobuchar, J.A. (leader) and Working Group, B. "Transionospheric propagation prediction s," in R.F. Donnelly (cd.), Vol. 2: Working Group Reports and Reviews of Solar-Terrestrial Predictions Proceedings,, Boulder, CO: Environmental Research Labs., NOAA, 1979.

Kobyashi, T., "Pre-estimation of cross-polarization discrimination due to rain, " J. Radio Res. Labs, (Japan), vol.23, pp. 47-64, March 1976.

Lee, M.C. et al., "Depolarization of VHF geostationary satellite signals near the equatorial anomaly crests, " Radio Sci., vol. 17, p.399-409, March-April 1982.

Lee, W.C. Y., "An approximate method for obtaining rain statistics for use in sigal attenuation estimating," IEEE Trans. Antennas Propagat., vol. AP-27, pp.407-413, May 1979.

Malin, S.R.C. and D.R. Barraclough, "An algorithm for synthesizing the geostationary field," Comput. Geosci., vol. 7, No. 4, pp. 401-405, 1981.

McEwan, N.J. et al., "Crosspolarization from high altitude hydrometeors on a 20 GHz satellite radio path," Electronics Lett., vol. 13, pp .13-14, 1977.

Millman, G.H. and G.M. ReinSmith, An Analysis of the Incoherent Scatter Faraday Rotation Technique for Ionospheric Propagation Error Correction (R 74EMH2). Syracuse, NY: General lectric, Feb. 1974.

Millman, G. H., Ionospheric Electron Content Effects on Earth-Space Radio Propagation (R80EMH11). Syracuse, NY: General Electric, Dec. 1980.

Minakoshi, H. et al., "Severe ionospheric scintillation associated with magnetic storm on March 22, 1979 ," J. Radio Res. Labs. (Japan), vol. 28, pp. 1-9, March-July 1981.

Mullen, J.P. et al., "UHF/GHz scintillation observed at Ascension Island from 1980 through 1982," Radio Sci., vol. 20, pp. 357-365, May-June 1985.

Njoko, E.G. and E.K. Smith, "Microwave antenna temperature of the earth from geostationary orbit ," Radio Sci., vol. 20, pp. 591-599, May-June 1985.

Olsen, R. L., D.V. Rogers, and D.B. Hedge, "The aR^b relation in the calculation of rain attenuation," IEEE Trans. Antennas Propagat., vol. AP-26, pp. 318-329, March 1978.

Segal, B, "The influence of- raingauge integration time on measured rainfall-intensity, distribution functions," J. Atmospheric Oceanic Tech., vol. 3, Dec. 1986.

Sobin, S, D., Microwave Noise Temperature and Attenuation of Clouds at Frequencies Below 50 GHz, JPL Pub. 81-46. Pasadena, CA: Jet 'Propulsion Lab., 1981.

Sobin, S. D., "Microwave noise temperature and attenuation of clouds: statistics of these effects ar various sites in the United States, Alaska, and Hawaii," Radio Sci., vol. 17, pp. 1443-1454. Nov.-Dee. 1982.

Smith, E. K., "Centimeter and millimeter wave attenuation and brightness temperature due to atmospheric oxygen and water vapor, " Radio Sci., vol. 17, pp. 1455-1464, Nov.-Dee. 1982.

Strickland, J. I., R.I. Olsen, and H.L. Werstivk, "Measurements on low angle fading in the Canadian Arctic," Ann. Telecomm., vol. 32, pp. 530-535, 1977.

Taur, R. R., "Rain depolarization measurements on a satellite-earth propagation path at 4 GHz," IEEE Trans. Antennas Propagat., vol. 23, pp. 854-858, Nov. 1975.

Thompson, M. C., L.E. Wood, H.B. Janes, and D. Smith, "Phase and amplitude scintillations in the 10 to 40 GHz band," IEEE Trans. Antennas Propagat., vol. AP-23, pp. 792-797, Nov. 1975.

Titheridge, J. E., "Determination of ionospheric electron content from the Faraday rotation of geostationary satellite signals," Planet. Space Sci., vol. 20, pp. 353-369, 1972.

Vogel, W. J., G.W. Torrence, J. Goldhirsh, and J.R. Rowland, "Propagation considerations for land mobile satellite service: signal characteristics in mountainous terrain at UHF and L band," National Radio Science Meeting (URSI), 12-15 Jan. 1987, Boulder, CO.

APPENDIX 9.1

DETERMINATION OF B_L USING DIPOLE MODEL

In this appendix, a procedure is described for determining a value of B_L for estimating Faraday rotation as a function of ionospheric TEC. The procedure can be applied to any ionospheric height; we use a height of 400 km in the absence of information pointing to a different choice. For a particular earth-station location and path, the geographic latitude and longitude of the intersection of the path with the 400-km height level can be determined by the use of spherical triginometry.

The dipole model may be described by assuming a scalar magnetic potential V given by $V = -M (\cos \theta)/r^2$, where M is dipole magnetic moment, θ is the angle measured from the dipole axis, and r is the distance from the center of the Earth. Then $F = -VV$, where F is the total magnetic flux density vector and has a vertical component Z given by $Z = \partial V/\partial r = 2M (\cos \theta)/r^3$ and a horizontal component H given by $H = (1/r) \partial V/\partial \theta = M (\sin \theta)/r^3$. The dipole axis should ideally pass through the observed north and south magnetic dip poles but their positions, which vary with time, are not directly opposite from each other or consistent with a purely dipole field, The north magnetic pole is near Ellef Ringnes Island in the Canadian arctic. The axis of the dipole model that best approximates the observed field overall intersects the Earth's surface at a different location, namely the north geomagnetic pole. The north geomagnetic pole is in Greenland, very close to the northwest coast. Its postion was taken to be 78.3 deg N and 69 deg W in 1965 (Davies, 1965). In a 1982 paper on the magnetic poles of the Earth, Dawson and Newitt (1982) give values of 78.8 deg N and 70.9 deg W.

Rather than specifying a value for M, the magnetic moment, the expression for Z and H can be given in terms of B_o, the magnetic flux density at the Earth's surface at the geomagnetic equator. The expressions then become

$$Z = 2 B_o (a/r)^3 \cos \theta \qquad \text{(A9.1)}$$

and

$$H = B_o (a/r)^3 \sin \theta \qquad \text{(A9.2)}$$

with

$$F = (H^2 + Z^2)^{1/2} \qquad \text{(A9.3)}$$

where a is the Earth's radius (mean value about 6371 km). Substituting the expression for H and Z into Eq. (A9. 3), it becomes

$$F = B_{\sim} (a/r)^3 (\sin^2\theta + 4\cos^2\theta)^{1/2}$$

$$= B. (a/r)^3 (\sin^2\theta + 3\cos^2\theta + 1 - \sin^2\theta)^{1/2}$$

$$= B_0 (a/r)^3 (1 + 3\,\mathrm{Cos}^2\theta)^{1/2} \qquad \text{(A9.4)}$$

Equations (A9. 1), (A9.2), and (A9.4) refer to the angle θ measured from the polar axis, but for some purposes it is more convenient to use the magnetic latitude 0', which is measured from the magnetic equator. In terms of latitude 6', the expressions become

$$Z = 2 B. (a/r)^3 \sin\theta' \qquad \text{(A9.5)}$$

$$H = B. (a/r)^3 \cos\theta' \qquad \text{(A9.6)}$$

$$F = B (a/r)^3 (1 + 3\sin^2\theta')^{*'^2} \qquad \text{(A9.7)}$$

If in Eq. (A9.7) F is held constant, it develops that the radial coordinate r corresponding to a particular value of F is given by

$$r = (B_0/F)^{1/3} a (1 + \sin^2\theta')^{1/6} \qquad \text{(A9.8)}$$

The quantity -F represents the magnitude of the total magnetic flux density. To obtain a plot showing the direction of the magnetic flux density vector (showing magnetic flux lines), note that the direction of the vector at a particular point is as indicated by

$$\frac{dr}{r\,d\theta} = \frac{z}{H} \qquad \text{(A9.9)}$$

where an increment of length along a field line, dl, has a component dr in the radial direction and a component $rd\theta$ in the horizontal direction. Rearranging Eq. (A9.9) leads to

$$dr/r = (Z/H)\,d\theta = 2\cot\theta\,d\theta \qquad \text{(A9.1O)}$$

Integrating this expression from the point on the geomagnetic equator where r = ka to r = r and from $\theta = \pi/2$ to θ

$$\int_{ka}^{r} \frac{dr}{r} = \int_{\pi/2}^{\theta} 2 \cot \theta \, d\theta$$

and

$$\ln (r/ka) = 2 \ln \sin \theta = \ln \sin^2\theta$$

from which

$$r = ka \sin^2\theta \qquad \text{(A9.11)}$$

or, in terms of latitude θ'

$$r = ka \cos^2\theta' \qquad \text{(A9.12)}$$

Note that a particular field line that crosses the equator at r = ka will intersect the Earth's surface at $\cos \theta' = (1/k)^{1/2}$.

An additional parameter describing the Earth's magnetic field is the dip angle I which can be determined from

$$\tan I = Z/H = 2 \cot \theta = 2 \tan \theta' \qquad \text{(A9.13)}$$

To estimate the value of B_L for a particular path, one needs to determine the geographic coordinates of the point where the path intersects the 400-km height level. To make this determination, use can be made of Fig. A9. 1 which is like Fig. 1.1 but with an additional radial line passing through the 400 km intercept at Z'. Also ψ of Fig. i. 1 is at its minimum value of 90 deg in Fig. A9. 1.

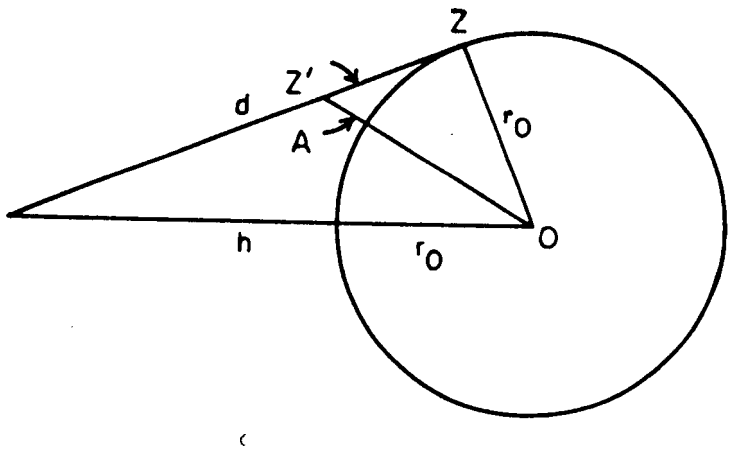

Figure A9. 1. Geometry for determination of Z'.

The law of sines can be applied to the triangle 22'0 resulting in

$$\frac{\sin \psi}{r. + 400} \qquad \frac{\sin A}{r_0} \qquad \frac{\sin [\ 180° - \psi (z - Z')]}{r_0} \tag{A9. 14}$$

The angle ψ can be calculated by use of Eqs. (1. 13) and (1. 15) and then 2', the only remaining unknown in Eq. (A9. 14) , can be determined. If the satellite and earth station are at the same longitude, **Z** is the latitude of the earth station and **Z'** is the latitude of the 400-km intercept. If the satellite and earth station are not on the same longitude, both the latitude and longitude of **Z'** are different from those of **Z.** The latitude and longitude of **Z'** can be determined by referring to spherical triangles like those of Fig. 1.2, a reference triangle showing Z and a smaller triangle for Z', with **Z'** a shorter distance from the subsatellite point than Z. In particular one can use

$$\sin \phi' = \sin Z' \sin \alpha \tag{A9.15}$$

and

$$\sin \theta' = \tan \phi' \cot \alpha \tag{A9.16}$$

where α is determined by use of Eq. (1.17). Note that the two triangles are like two plane triangles in that the angle α is the same for both. Also note the θ' is latitude, an angle measured from the equator, whereas ϕ' is an angle measured from the subsatellite point and not longitude but a difference in longitude.

Having the geographic coordinates of the earth station, the 400-km intercept, and the satellite, one can obtain the corresponding geomagnetic coordinates by use of

$$\sin \theta'_m = \sin \theta'_g \sin e' + \cos e' \cos \theta'_p \cos (\phi_g - \phi_p) \tag{A9.17}$$

and

$$\sin \phi_m = \frac{\cos \theta'_g \sin (\phi_g - \phi_p)}{\cos \theta'_m} \tag{A9.18}$$

where the primes represent latitudinal quantities, θ'_m is the magnet ic latitude of the location of interest, θ'_g is its geographic

latitude, θ'_p is the geographic latitude of the north geomagnetic pole, $\#_m$ is the' magnetic longitude of the location of interest, $\#_g$ is its geographic longitude, and ϕ_p is the geographic longitude of the north geographic pole.

Having expressed all quantities in magnetic coordinates [previously the subscript m was not used but Eqs. (A9. 1) to (A9. 13) are all in magnetic coordinates], one can obtain vector representations of d, the path from the earth station to the satellite and F, the total geomagnetic field at the 400-km intercept. One can then determine the angle between the magnetic field and the path at 400 km by using

$$Fd \cos \theta_B = F \cdot d \qquad \text{(A9.19)}$$

where θ_B is the angle desired and $F \cdot d$ is the scalar dot product of vectors. The magnetic field F and the locations of the satellite (S) and the earth station (G) can be most conveniently described in spherical coordinates initially, but to find d = S - G and to take the dot product they are converted to rectangular coordinates by use of

$$a_r = \sin\theta \cos\phi\, a_x + \sin\theta \sin\phi\, a_Y + \cos\theta\, a_z \qquad \text{(A9.20)}$$

$$a_\theta = \cos\theta \cos\phi\, a_x + \cos\theta \sin\phi\, a_Y - \sin\theta\, a_z \qquad \text{(A9.21)}$$

for F and

$$x = r \sin e \cos\phi \qquad \text{(A9.22)}$$

$$Y = r \sin\theta \sin\phi \qquad \text{(A9.23)}$$

$$z = r \cos e \qquad \text{(A9.24)}$$

for the locations of the earth station and satellite. Note that in these expression θ is colatitude, the polar angle of spherical coordinates, rather than latitude 0'. Once the magnitude of F and the angle θ_B are known, one has B_L from

$$'L = F \cos\theta_B \qquad \text{(A9.25)}$$